

HD-TVP-95-06

# Hadronization in the

## $SU(3)$ Nambu–Jona–Lasinio Model

P. Rehberg\*, S. P. Klevansky and J. Hüfner

*Institut für Theoretische Physik, Universität Heidelberg,  
Philosophenweg 19, D-69120 Heidelberg, Germany*

(June 1995)

### Abstract

The hadronization process for quarks combining into two mesons,  $q\bar{q} \rightarrow MM'$  at temperature  $T$  is described within the  $SU(3)$  Nambu–Jona–Lasinio model with finite current quark masses. Invariant matrix elements, cross–sections and transition rates are calculated to leading order in a  $1/N_c$  expansion. Four independent classes,  $u\bar{d}$ ,  $u\bar{s}$ ,  $u\bar{u}$  and  $s\bar{s} \rightarrow$  hadrons are analysed, and the yield is found to be dominated by pion production. Threshold behaviour is determined by the exothermic or endothermic nature of the processes constituting the hadronization class. A strong suppression of transition rates is found at the pionic Mott temperature  $T_{M\pi} = 212$  MeV, at which the pion becomes a resonant state. The mean time for hadronization is calculated to be 2–4 fm/ $c$  near the Mott temperature. The calculation of strangeness changing processes indicates that hadronization accounts for a 1% increase in the absolute value of the kaon to pion ratio at  $T = 150$  MeV.

PACS numbers: 11.30Rd, 12.39.Fe, 13.60.Le, 24.85.+p

Typeset using REVTeX

---

\*E-Mail: Peter@Frodo.TPhys.Uni-Heidelberg.DE

## I. INTRODUCTION

One of the current outstanding problems facing nuclear and particle theoreticians today lies in understanding the phase transition from a constituent quark and gluonic matter to that of observed hadronic matter. Since it is expected firstly that such a deconfined state of quarks and gluons exists, and secondly that it may be observed via  $Pb + Pb$  and other heavy ion collisions already and also to be undertaken at CERN, an adequate description of the hadronization process that leads one from the quark and gluon degrees of freedom inherent to QCD to the observed hadron spectrum is really required. The present state of the art (for an overview over the field see the proceedings of the Quark Matter conferences [1,2] or the book [3]) is characterized either by phenomenological approaches for the parton to hadron transition [4,5] or computer codes based on string phenomenology [6].

In this paper, we place our emphasis on describing the hadronization process of quarks and antiquarks into two mesons, within a microscopic, field theoretical, and non-perturbative framework, which is carried through at finite temperatures. In itself this is a demanding project that cannot yet be performed directly starting from the QCD Lagrangian, and thus the price that we have to pay is in making a choice of a *model* Lagrangian. To this end, we invoke the Nambu–Jona–Lasinio (NJL) model [7–9] in its  $SU_L(3) \times SU_R(3)$  version, which has been constructed to display the same internal symmetries as QCD itself. This model is known to provide a good description of the static properties pertaining to both the nonstrange and strange meson sector at zero temperature, and it allows for a transparent description at finite temperatures, explicitly displaying the chiral symmetry restoration phase transition at a critical temperature of about 200 MeV in the chiral limit. Although we are aware of the deficiencies of the model — lack of confinement as well as non-renormalizability in a strict field theoretic sense — it nevertheless is possible to construct a comprehensive physical picture from the calculations performed to date both at  $T = 0$  and at finite temperatures and densities. For definiteness, it is useful to argue from the chiral limit. Assuming that the chiral and deconfinement phase transitions occur at the same temperature — an assumption supported by lattice gauge simulations [10] — one can build a heuristic picture on the basis of the NJL model. At  $T \geq T_c$ , hadronic states are unstable, and the system is dominated

by interacting quarks with constituent mass  $m = 0$ . For  $T \leq T_c$ , where chiral symmetry is broken,  $m \neq 0$ ,  $m_\pi = 0$ ,  $m_\sigma = 2m$ , and a *plasma* of quarks and mesons is formed. While the appearance of quarks for temperatures  $T \leq T_c$  is an artifact of the model due to the absence of confinement, the situation for  $T \geq T_c$  is realistic, except for the lack of explicit gluonic degrees of freedom. As such, however, the process of hadronization may be reliable around the critical temperature, where the shortcomings of the model may not be too severe. These arguments can be extended to the physical case of non-zero current quark masses, which we in fact study here.

The purpose of this paper is thus to investigate all hadronization processes of the type  $q\bar{q} \rightarrow MM'$ , where  $M$  represents a meson in the non-strange or strange sector, and here  $q = u, d, s$ . In particular, we evaluate scattering amplitudes and cross-sections, and study the hadronization rates for all these processes, which in turn are necessary elements for constructing a dynamical non-equilibrium transport theory for this model Lagrangian [11]. This should aid us in understanding the role that chiral symmetry plays in dynamical processes. Our approach follows in part, and develops further the calculation performed in  $SU(2)$  in the chiral limit described in the letter [12].

In our study of the  $SU(3)$  sector, we classify hadronization processes according to the incoming quark and antiquark, finding a total of four independent classes under the additional assumption of  $SU(2)$  isospin symmetry, where  $m_u = m_d$ . We thus consider the processes with  $u\bar{d}$ ,  $u\bar{s}$ ,  $u\bar{u}$  and  $s\bar{s}$  as incoming pairs, which we also list. The mesons  $M$  and  $M'$  considered in the process are  $\pi$ ,  $K$  and  $\eta$ , which are the stable ones with respect to the strong interaction. Feynman diagrams for the scattering amplitudes pertaining to these reactions have a generic form which describes all  $q\bar{q} \rightarrow MM'$ . We select the diagrams according to an expansion in the inverse number of colors in the model,  $1/N_c$ , that is commensurate with the Hartree approximation for the self-energy and the random phase approximation for the scattering amplitude [13–15]. The variations in applying each of the Feynman diagrams to the different scattering channels arise from differing exchanged mesons, quark masses and flavor factors. We choose to illustrate our calculation by analytically constructing the formulae for the cross sections of the processes  $u\bar{d} \rightarrow \pi^+\pi^0$ ,  $u\bar{s} \rightarrow \pi^+\overline{K^0}$  and  $u\bar{u} \rightarrow \pi^+\pi^-$ . The first of these explicitly includes a  $u$  channel exchange, while the second has unequal masses for all incoming and outgoing particles. The final process

illustrates the role of the mixing of the scalar mesons in the  $SU(3)$  Lagrangian due to the t'Hooft term and the differing up, down and strange quark masses.

All quantities are calculated as a function of temperature and baryonic chemical potential. It turns out that a cardinal role is played by the Mott temperatures,  $T_{M\pi}$ ,  $T_{M\sigma}$ ,  $T_{MK}$ ,  $T_{M\eta}$ , that are defined to be the temperatures at which the masses of the respective mesons  $\pi$ ,  $\sigma$ ,  $K$ ,  $\eta$ , are equal to the sum of the masses of their constituents. Note that these four mesons are bound states at  $T = 0$ . At the Mott temperatures, the respective meson–quark couplings go to zero, and this in turn influences the transition amplitudes and transition rates in that they are suppressed. In particular the pionic Mott temperature plays the dominant role, driving the total transition rates (almost) to zero at this point. We comment that the use of a finite temperature explicitly breaks Lorentz invariance in our calculation. We do not attempt to resolve this problem here. Quantities are simply calculated with respect to the rest frame of the medium.

In order to make a connection with transport theory, we calculate transition rates, which are constructed by multiplying the total cross section of a particular process with the relative velocity. Our numerical results indicate that in a per-channel calculation, the  $t$  and  $u$  channel exchange of any one process dominate over the  $s$  channel exchange, except perhaps in an energy range where a resonance is present. The  $t$  and  $u$  channel graphs, if present in a process, give cancelling contributions at threshold when the flavor factors are equal. In dealing with the four independent hadronization classes, we are directly able to identify the leading contributions at all energies. These, with the exception of the  $s\bar{s}$  hadronization class, are dominated by pion production. The  $s\bar{s}$  processes on the other hand are found to be dominated by kaon production. In all these calculations we can confirm that the exothermic reactions are always dominant over the endothermic ones, as far as they are present.

We also examine the energy averaged transition rates. These quantities, multiplied by the density of incoming quarks, can be interpreted as the inverse of the hadronization time. We find this to be of the order of  $\tau = 2\text{--}4\text{ fm}/c$  in the temperature range 160–200 MeV, rising rapidly as one moves towards the pion Mott temperature  $T_{M\pi}$ , or to lower temperatures. This indicates that hadronization occurs preferentially over this given range of temperatures within our model.

Finally we have also examined processes that change the number of  $s$  plus  $\bar{s}$  quarks, like e. g.  $u\bar{d} \rightarrow K^+\bar{K}^0$ . We find that the hadronization process generates an enhancement of 1% in the absolute value of the ratio of kaons to pions at  $T = 150$  MeV. This is to be compared with the experimental value of  $(15.4 \pm 0.8)\%$  for the  $K/\pi$  ratio found for  $S + S$  collisions, which itself constitutes an enhancement of 9% over the  $N + N$  value of  $(6.5 \pm 1.1)\%$  [16].

In order to facilitate the technical evaluation, we decompose all quantities into fundamental integrals containing one, two or three denominators, and which arise for instance from the self-energy, polarization and the three meson vertex. In principle, these functions can be calculated for arbitrary values of the differing quark masses and associated differing chemical potentials. In this way, general expressions can be constructed if one utilizes the modular forms. For actual calculational purposes, however, we will set all chemical potentials to zero, and study temperature and energy dependencies here, giving some relevant analytical results for these integrals in an appendix.

This paper is structured as follows: In Section II, we discuss the general  $SU_L(3) \times SU_R(3)$  Lagrangian that we use, and give the relevant functions associated with the mass spectrum evaluation that we require. In particular the  $\eta-\eta'$  mixing is detailed, and the scalar resonance sector, which plays the role of intermediate states in the hadronization. In Section III, the possible hadronization processes are classified, and the explicit examples  $u\bar{d} \rightarrow \pi^+\pi^0$ ,  $u\bar{s} \rightarrow \pi^+K^0$  and  $u\bar{u} \rightarrow \pi^+\pi^-$  are discussed. Numerical results for the transition rates for each hadronization class are given in Section IV. Strangeness changing processes are also analyzed here. We summarize and conclude in Section V.

## II. PROPERTIES OF MESONS IN $SU(3)$

### A. General Considerations

This section serves to introduce our Lagrange density and notation, commencing with the three flavor Lagrangian

$$\mathcal{L} = \sum_{f=0}^3 \bar{\psi}_f (i\cancel{\partial} - m_{0f}) \psi_f$$

$$\begin{aligned}
& + G \sum_{a=0}^8 \left[ (\bar{\psi} \lambda^a \psi)^2 + (\bar{\psi} i \gamma_5 \lambda^a \psi)^2 \right] \\
& - K \left[ \det \bar{\psi} (1 + \gamma_5) \psi + \det \bar{\psi} (1 - \gamma_5) \psi \right] \quad ,
\end{aligned} \tag{1}$$

where  $G$  and  $K$  are dimensionful coupling strengths. The term containing  $G$  displays  $U(3) \times U(3)$  symmetry, while the determinantal term controlled by  $K$  breaks this down to  $SU(3) \times SU(3)$ . Flavor and color indices have been suppressed for convenience in the interaction terms. However, the flavor indices have been *explicitly* included in the first term, since the current quark masses  $m_{0f}$ , that themselves explicitly break the  $SU(3) \times SU(3)$  symmetry, are regarded as distinct. For general reviews on the three flavor version of the NJL model, the reader is referred to Refs. [7–9].

It is useful to convert the determinantal term in Eq. (1) into an effective two-body term in the mean field approximation. This follows on contracting out one pair of quark and antiquark fields and dividing this result by two. One may recombine the result with the existing two body term that is controlled by  $G$  to find the effective Lagrangian to be

$$\begin{aligned}
\mathcal{L} = & \sum_{f=0}^3 \bar{\psi}_f (i \not{d} - m_{0f}) \psi_f \\
& + \sum_{a=0}^8 \left[ K_a^- (\bar{\psi} \lambda^a \psi)^2 + K_a^+ (\bar{\psi} i \gamma_5 \lambda^a \psi)^2 \right] \\
& + K_{30}^- (\bar{\psi} \lambda^3 \psi) (\bar{\psi} \lambda^0 \psi) + K_{30}^+ (\bar{\psi} i \gamma_5 \lambda^3 \psi) (\bar{\psi} i \gamma_5 \lambda^0 \psi) \\
& + K_{03}^- (\bar{\psi} \lambda^0 \psi) (\bar{\psi} \lambda^3 \psi) + K_{03}^+ (\bar{\psi} i \gamma_5 \lambda^0 \psi) (\bar{\psi} i \gamma_5 \lambda^3 \psi) \\
& + K_{80}^- (\bar{\psi} \lambda^8 \psi) (\bar{\psi} \lambda^0 \psi) + K_{80}^+ (\bar{\psi} i \gamma_5 \lambda^8 \psi) (\bar{\psi} i \gamma_5 \lambda^0 \psi) \\
& + K_{08}^- (\bar{\psi} \lambda^0 \psi) (\bar{\psi} \lambda^8 \psi) + K_{08}^+ (\bar{\psi} i \gamma_5 \lambda^0 \psi) (\bar{\psi} i \gamma_5 \lambda^8 \psi) \\
& + K_{83}^- (\bar{\psi} \lambda^8 \psi) (\bar{\psi} \lambda^3 \psi) + K_{83}^+ (\bar{\psi} i \gamma_5 \lambda^8 \psi) (\bar{\psi} i \gamma_5 \lambda^3 \psi) \\
& + K_{38}^- (\bar{\psi} \lambda^3 \psi) (\bar{\psi} \lambda^8 \psi) + K_{38}^+ (\bar{\psi} i \gamma_5 \lambda^3 \psi) (\bar{\psi} i \gamma_5 \lambda^8 \psi)
\end{aligned} \tag{2}$$

with the effective coupling constants

$$K_0^\pm = G \mp \frac{1}{3} N_c K (i \text{tr}_\gamma S^u(x, x) + i \text{tr}_\gamma S^d(x, x) + i \text{tr}_\gamma S^s(x, x)) \tag{3a}$$

$$K_1^\pm = K_2^\pm = K_3^\pm = G \pm \frac{1}{2} N_c K i \text{tr}_\gamma S^s(x, x) \tag{3b}$$

$$K_4^\pm = K_5^\pm = G \pm \frac{1}{2} N_c K \text{itr}_\gamma S^d(x, x) \quad (3c)$$

$$K_6^\pm = K_7^\pm = G \pm \frac{1}{2} N_c K \text{itr}_\gamma S^u(x, x) \quad (3d)$$

$$K_8^\pm = G \pm \frac{1}{6} N_c K (2 \text{itr}_\gamma S^u(x, x) + 2 \text{itr}_\gamma S^d(x, x) - \text{tr}_\gamma S^s(x, x)) \quad (3e)$$

$$K_{03}^\pm = K_{30}^\pm = \mp \frac{1}{2\sqrt{6}} N_c K (\text{itr}_\gamma S^u(x, x) - \text{itr}_\gamma S^d(x, x)) \quad (3f)$$

$$K_{08}^\pm = K_{80}^\pm = \pm \frac{\sqrt{2}}{12} N_c K (\text{itr}_\gamma S^u(x, x) + \text{itr}_\gamma S^d(x, x) - 2 \text{itr}_\gamma S^s(x, x)) \quad (3g)$$

$$K_{38}^\pm = K_{83}^\pm = \pm \frac{1}{2\sqrt{3}} N_c K (\text{itr}_\gamma S^u(x, x) - \text{itr}_\gamma S^d(x, x)) \quad . \quad (3h)$$

In Eq. (3),  $\text{tr}_\gamma$  refers to the spinor trace alone, while  $S^f$  is the diagonal quark propagator for a given flavor  $f$ , which, in the imaginary time formalism for finite temperatures can be written as

$$S^f(\vec{x} - \vec{x}', \tau - \tau') = \frac{i}{\beta} \sum_n e^{-i\omega_n(\tau - \tau')} \int \frac{d^3 p}{(2\pi)^3} \frac{e^{i\vec{p}(\vec{x} - \vec{x}')}}{\gamma_0(i\omega_n + \mu_f) - \vec{\gamma}\vec{p} - m_f} \quad . \quad (4)$$

Here the Matsubara frequencies are fermionic,  $i\omega_n = (2n + 1)\pi/\beta$ , with  $n = 0, \pm 1, \pm 2, \pm 3, \dots$ , and  $\mu_f$  is the chemical potential for a quark of flavor  $f$ .

As can be seen from Eqs. (2, 3), the nondiagonal coupling constants  $K_{03}^+$ ,  $K_{08}^+$  and  $K_{38}^+$  give rise to the  $\pi^0$ - $\eta$ - $\eta'$  mixing. If one assumes  $SU(2)$  isospin symmetry, i. e.  $m_u = m_d$ , then  $K_{03}^+$  and  $K_{38}^+$  vanish identically, with the consequence that the  $\pi^0$  decouples from the  $\eta$  and  $\eta'$ . We make this assumption in what follows, using the generic label  $q$  for  $u$ ,  $d$ , and always writing  $s$  explicitly.

Writing

$$i\text{tr}_\gamma S^f(x, x) = -\frac{m_f}{4\pi^2} A(m_f, \mu_f) \quad , \quad (5)$$

where

$$A(m_f, \mu_f) = \frac{16\pi^2}{\beta} \sum_n e^{i\omega_n \eta} \int_{|\vec{p}| < \Lambda} \frac{d^3 p}{(2\pi)^3} \frac{1}{(i\omega_n + \mu_f)^2 - E_f^2} \quad (6)$$

(with  $E_f^2 = p^2 + m_f^2$ ) denotes the first loop integral (cf. Appendix A), one can easily derive the coupled gap-equations

$$m_u = m_{0u} - \frac{GN_c}{\pi^2} m_u A(m_u, \mu_u) + \frac{KN_c^2}{8\pi^4} m_d m_s A(m_d, \mu_d) A(m_s, \mu_s) \quad (7a)$$

$$m_d = m_{0d} - \frac{GN_c}{\pi^2} m_d A(m_d, \mu_d) + \frac{KN_c^2}{8\pi^4} m_s m_u A(m_s, \mu_s) A(m_u, \mu_u) \quad (7b)$$

$$m_s = m_{0s} - \frac{GN_c}{\pi^2} m_s A(m_s, \mu_s) + \frac{KN_c^2}{8\pi^4} m_u m_d A(m_u, \mu_u) A(m_d, \mu_d) \quad (7c)$$

from the mean field or Hartree approximation to the self-energy, and which determine the physical quark masses.

## B. Pions and Kaons

Imposing the degeneracy condition  $m_u = m_d$ , the determination of both the pion and kaon masses follows similarly to the standard approach taken in the two flavor model [8]. This comes about, since the off-diagonal coupling strengths  $K_{03}^\pm$  and  $K_{38}^\pm$  are identically zero, and the  $\pi^0$  is decoupled from the  $\eta$  and  $\eta'$ . In this limit, the  $\pi^\pm, \pi^0$  become degenerate. Concomitantly,  $K_4^\pm = K_6^\pm$ , which means physically that neutral and charged kaons have the same mass.

The quark-quark scattering amplitude is calculated in the random phase approximation (RPA, see Fig. 1), which yields the result

$$M_\pi(k_0, \vec{k}) = \frac{2K_1^+}{1 - 4K_1^+ \Pi_{q\bar{q}}^P(k_0, \vec{k})} \quad (8)$$

for the pion scattering amplitude and

$$M_K(k_0, \vec{k}) = \frac{2K_4^+}{1 - 4K_4^+ \Pi_{q\bar{s}}^P(k_0, \vec{k})} \quad (9)$$

for the kaon one. Here  $\Pi^P(k_0, \vec{k})$  represents the irreducible pseudoscalar polarization (see Fig. 2), which, in the finite temperature Matsubara formalism, depends on  $k_0$  and  $\vec{k}$  separately, because the medium breaks Lorentz invariance. For arbitrary flavors, the irreducible polarization is given by the analytic continuation of the imaginary time form

$$\begin{aligned}
-i\Pi_{f_1f_2}^P(i\nu_m, \vec{k}) &= -N_c \frac{i}{\beta} \sum_n \int \frac{d^3p}{(2\pi)^3} \text{tr}_\gamma \left[ iS^{f_1}(i\omega_n, \vec{p}) i\gamma_5 iS^{f_2}(i\omega_n - i\nu_m, \vec{p} - \vec{k}) i\gamma_5 \right] \\
&= 4iN_c \frac{1}{\beta} \sum_n \int \frac{d^3p}{(2\pi)^3} \frac{(i\omega_n + \mu_1)(i\omega_n - i\nu_m + \mu_2) - \vec{p}(\vec{p} - \vec{k}) - m_1 m_2}{[(i\omega_n + \mu_1)^2 - E_1^2][(i\omega_n - i\nu_m + \mu_2)^2 - E_2^2]} \quad (10)
\end{aligned}$$

where  $E_1 = \sqrt{\vec{p}^2 + m_1^2}$ ,  $E_2 = \sqrt{(\vec{p} - \vec{k})^2 - m_2^2}$ , and the mesonic Matsubara frequencies  $i\nu_m = 2m\pi/\beta$  are even,  $m = 0, \pm 1, \pm 2, \dots$ . Note that the irreducible polarization in this definition does not contain any flavor factors from the Gell-Mann  $\lambda$ -matrices. These factors are incorporated explicitly in Eqs. (8, 9) as multiplicative cofactors of the coupling and polarization.

We may decompose  $\Pi^P(k_0, \vec{k})$  in terms of the function  $A(m, \mu)$  already defined in Eq. (6) as

$$\begin{aligned}
\Pi^P(k_0, \vec{k}) &= -\frac{N_c}{8\pi^2} \left[ A(m_1, \mu_1) + A(m_2, \mu_2) \right. \quad (11) \\
&\quad \left. + \left( (m_1 - m_2)^2 - (k_0 + \mu_1 - \mu_2)^2 + \vec{k}^2 \right) B_0(\vec{k}, m_1, \mu_1, m_2, \mu_2, k_0) \right] ,
\end{aligned}$$

introducing the second loop integral (cf. Appendix A)

$$\begin{aligned}
B_0(\vec{k}, m_1, \mu_1, m_2, \mu_2, i\nu_m) &= \quad (12) \\
\frac{16\pi^2}{\beta} \sum_n e^{i\omega_n \eta} \int_{|\vec{p}| < \Lambda} \frac{d^3p}{(2\pi)^3} \frac{1}{((i\omega_n + \mu_1)^2 - E_1^2)} \frac{1}{((i\omega_n - i\nu_m + \mu_2)^2 - E_2^2)} &.
\end{aligned}$$

(Note that in Eq. (11), an analytic continuation has been performed.) We comment that, due to rotational invariance,  $B_0$  does not fully depend on  $\vec{k}$ , but only on  $|\vec{k}|$ .

In terms of the modular integrals,  $A$  and  $B_0$ , polarizations required can then be explicitly given for arbitrary chemical potential and temperature as

$$\Pi_{q\bar{q}}^P(k_0, \vec{k}) = -\frac{N_c}{8\pi^2} \left[ 2A(m_q, \mu_q) - k^2 B_0(\vec{k}, m_q, \mu_q, m_q, \mu_q, k_0) \right] \quad (13)$$

$$\Pi_{s\bar{s}}^P(k_0, \vec{k}) = -\frac{N_c}{8\pi^2} \left[ 2A(m_s, \mu_s) - k^2 B_0(\vec{k}, m_s, \mu_s, m_s, \mu_s, k_0) \right] \quad (14)$$

$$\begin{aligned}
\Pi_{q\bar{s}}^P(k_0, \vec{k}) &= -\frac{N_c}{8\pi^2} \left[ A(m_q, \mu_q) + A(m_s, \mu_s) \right. \quad (15) \\
&\quad \left. + \left( (m_q - m_s)^2 - (k_0 + \mu_q - \mu_s)^2 + \vec{k}^2 \right) B_0(\vec{k}, m_q, \mu_q, m_s, \mu_s, k_0) \right] .
\end{aligned}$$

The pion and kaon masses are determined according to the dispersion relations [8]

$$1 - 4K_1^+ \Pi_{q\bar{q}}^P(m_\pi, \vec{0}) = 0 \quad (16)$$

$$1 - 4K_4^+ \Pi_{q\bar{s}}^P(m_K, \vec{0}) = 0 \quad , \quad (17)$$

while effective couplings can be identified from the pole approximation forms

$$M_\pi(k_0, \vec{k}) \approx \frac{-g_{\pi q\bar{q}}^2}{k^2 - m_\pi^2} \quad (18)$$

$$M_K(k_0, \vec{k}) \approx \frac{-g_{K q\bar{s}}^2}{k^2 - m_K^2} \quad (19)$$

to be

$$g_{\pi q\bar{q}}^{-2} = -\frac{1}{2m_\pi} \left. \frac{\partial \Pi_{q\bar{q}}^P(k_0, \vec{0})}{\partial k_0} \right|_{k_0=m_\pi} \quad (20)$$

$$g_{K q\bar{s}}^{-2} = -\frac{1}{2m_K} \left. \frac{\partial \Pi_{q\bar{s}}^P(k_0, \vec{0})}{\partial k_0} \right|_{k_0=m_K} \quad (21)$$

At low temperatures, Eqs. (16, 17) have bound state solutions with  $m_\pi < 2m_q$  and  $m_K < m_q + m_s$ . In this case, Eqs. (16, 17) are real equations. At higher temperatures, the polarization functions become complex functions with complex solutions for the meson masses, that we may write as [17]

$$m_\pi \rightarrow m_\pi - \frac{i}{2} \Gamma_\pi \quad (22)$$

$$m_K \rightarrow m_K - \frac{i}{2} \Gamma_K \quad . \quad (23)$$

Denoting the Mott transition temperatures  $T_{M\pi}$  and  $T_{MK}$  as the temperatures at which  $m_\pi = 2m_q$  and  $m_K = m_q + m_s$  respectively, one thus has the physical circumstance that at temperatures larger than  $T_{M\pi}$  or  $T_{MK}$ , respectively pions or kaons become resonances with finite widths due to the available decay channels into two quarks. From Eqs. (20, 21), it follows that the quark-meson couplings also become complex in this case.

### C. $\eta$ and $\eta'$

Because of the mixing terms occurring in Eq. (2), the calculation of the  $\eta$  and  $\eta'$  masses and couplings is somewhat more involved. The scattering amplitude is nondiagonal in this sector with entries  $M_{00}$ ,  $M_{88}$ , and  $M_{08} = M_{80}$ . Within the RPA, that is still expressed diagrammatically in Fig. 1, it can be calculated in matrix form to be [8]

$$M = 2K^+(1 - 2\Pi^P K^+)^{-1} , \quad (24)$$

where now  $K^+$  and  $\Pi^P$  are the  $2 \times 2$  matrices

$$K^+ = \begin{pmatrix} K_0^+ & K_{08}^+ \\ K_{80}^+ & K_8^+ \end{pmatrix} \quad (25)$$

$$\Pi^P = \begin{pmatrix} \Pi_0^P & \Pi_{08}^P \\ \Pi_{80}^P & \Pi_8^P \end{pmatrix} . \quad (26)$$

The  $K_i^+$  on the right hand side of Eq. (25) are as defined in Eqs. (3), while the pseudoscalar polarization functions are the linear combinations

$$\Pi_0^P = \frac{2}{3} (2\Pi_{q\bar{q}}^P + \Pi_{s\bar{s}}^P) \quad (27a)$$

$$\Pi_8^P = \frac{2}{3} (\Pi_{q\bar{q}}^P + 2\Pi_{s\bar{s}}^P) \quad (27b)$$

$$\Pi_{08}^P = \Pi_{80}^P = \frac{2\sqrt{2}}{3} (\Pi_{q\bar{q}}^P - \Pi_{s\bar{s}}^P) \quad (27c)$$

of the functions  $\Pi_{q\bar{q}}^P$  and  $\Pi_{s\bar{s}}^P$ , that can be evaluated via Eqs. (13, 14). In Eqs. (24) to (27), we have dropped the argument  $(k_0, \vec{k})$  for convenience. A determination of the masses and coupling strengths can be made on forming the inverse of the matrix  $M$ . We abbreviate this as

$$M^{-1} = \frac{1}{2\det K^+} \begin{pmatrix} \mathcal{A} & \mathcal{B} \\ \mathcal{B} & \mathcal{C} \end{pmatrix} \quad (28)$$

with

$$\mathcal{A} = K_8^+ - 2\Pi_0^P \det K^+ \quad (29a)$$

$$-\mathcal{B} = K_{08}^+ + 2\Pi_{08}^P \det K^+ \quad (29b)$$

$$\mathcal{C} = K_0^+ - 2\Pi_8^P \det K^+ \quad . \quad (29c)$$

Following [9], we introduce the diagonal forms  $M_\eta$  and  $M_{\eta'}$  via

$$M^{-1} = \frac{1}{4\det K^+} \begin{pmatrix} c & -s \\ s & c \end{pmatrix} \begin{pmatrix} M_\eta^{-1} & 0 \\ 0 & M_{\eta'}^{-1} \end{pmatrix} \begin{pmatrix} c & s \\ -s & c \end{pmatrix} \quad , \quad (30)$$

where it is a simple matter to verify that

$$M_\eta^{-1} = \mathcal{A} + \mathcal{C} - \sqrt{(\mathcal{A} - \mathcal{C})^2 + 4\mathcal{B}^2} \quad (31a)$$

$$M_{\eta'}^{-1} = \mathcal{A} + \mathcal{C} + \sqrt{(\mathcal{A} - \mathcal{C})^2 + 4\mathcal{B}^2} \quad (31b)$$

$$c^2 + s^2 = 1 \quad (32a)$$

$$c^2 - s^2 = \frac{\mathcal{C} - \mathcal{A}}{\sqrt{(\mathcal{A} - \mathcal{C})^2 + 4\mathcal{B}^2}} \quad (32b)$$

$$2cs = \frac{-2\mathcal{B}}{\sqrt{(\mathcal{A} - \mathcal{C})^2 + 4\mathcal{B}^2}} \quad . \quad (32c)$$

The masses of the  $\eta$  and  $\eta'$  mesons can now be determined via the condition

$$M_\eta^{-1}(m_\eta, \vec{0}) = 0 \quad (33)$$

$$M_{\eta'}^{-1}(m_{\eta'}, \vec{0}) = 0 \quad . \quad (34)$$

For meson masses that lie below the quark-antiquark mass threshold, these equations are again real. In practice, actual numerical determinations place the  $\eta$  mass below this threshold at  $T = 0$ , and at a specific Mott transition temperature  $T_{M\eta}$ , this becomes a resonance, in much the same way as occurs for the pions and kaons.

The  $\eta'$  meson, however, is distinguished by the fact that it *always* lies above the quark–antiquark threshold, and it therefore is a resonant state at all temperatures. Since this is an artifact due to the lack of confinement, we regard this feature with some scepticism. We nevertheless calculate its contribution to the relevant hadronization cross sections and transition rates, and find that it is negligible, so that it can be safely discarded.

To calculate the coupling constants from Eq. (28), we express  $M$  directly as

$$M = \frac{2}{\mathcal{D}} \begin{pmatrix} \mathcal{C} & -\mathcal{B} \\ -\mathcal{B} & \mathcal{A} \end{pmatrix} \quad (35)$$

with

$$\begin{aligned} \mathcal{D} &= (\mathcal{A}\mathcal{C} - \mathcal{B}^2) / \det K^+ \\ &= 1 - 2\text{tr}(\Pi K^+) + 4 \det \Pi \det K^+ \quad . \end{aligned} \quad (36)$$

At  $(k_0, \vec{k}) = (m_\eta, \vec{0})$ ,  $\mathcal{D} = 0$ , and in the usual fashion, we make a pole approximation giving the form

$$M = \frac{4m_\eta}{\frac{\partial \mathcal{D}}{\partial k_0} \Big|_{k_0=m_\eta}} \frac{1}{k^2 - m_\eta^2} \begin{pmatrix} \mathcal{C} & -\mathcal{B} \\ -\mathcal{B} & \mathcal{A} \end{pmatrix} \quad (37)$$

From this, one obtains

$$M_{ab} = -\frac{g_{a\eta}g_{b\eta}}{k^2 - m_\eta^2} \quad (38)$$

with

$$g_{0\eta}^2 = -\frac{4m_\eta \mathcal{C}}{\frac{\partial \mathcal{D}}{\partial k_0} \Big|_{k_0=m_\eta}} \quad (39)$$

$$g_{8\eta}^2 = -\frac{4m_\eta \mathcal{A}}{\frac{\partial \mathcal{D}}{\partial k_0} \Big|_{k_0=m_\eta}} \quad (40)$$

$$g_{0\eta}g_{8\eta} = \frac{4m_\eta \mathcal{B}}{\frac{\partial \mathcal{D}}{\partial k_0} \Big|_{k_0=m_\eta}} \quad . \quad (41)$$

From these coupling constants we may calculate [9]

$$g_{\eta q\bar{q}} = \sqrt{\frac{2}{3}}g_{0\eta} + \frac{1}{\sqrt{3}}g_{8\eta} \quad (42)$$

$$g_{\eta s\bar{s}} = \sqrt{\frac{2}{3}}g_{0\eta} - \frac{2}{\sqrt{3}}g_{8\eta} \quad . \quad (43)$$

The coupling strengths  $g_{\eta' q\bar{q}}$  and  $g_{\eta' s\bar{s}}$  may be evaluated in the same fashion. The set of couplings  $g_{\eta q\bar{q}}$ ,  $g_{\eta s\bar{s}}$  and  $g_{\eta' q\bar{q}}$ ,  $g_{\eta' s\bar{s}}$  enter directly into the cross section calculations.

#### D. Scalar Resonances

Since scalar mesons may occur as possible intermediate resonance structures in the hadronization cross sections, we are also interested in obtaining their masses. In contrast to the two flavor model, in which only the  $\sigma$  is present, we deal here with nine scalar resonances: three  $\sigma_\pi$ 's, which are the scalar partners of the pions, four  $\sigma_K$ 's, being the scalar partners of the kaons, and the  $\sigma$  and  $\sigma'$ , that are associated similarly with the  $\eta$  and  $\eta'$ . As occurs in the pseudoscalar case, for  $m_u \neq m_d \neq m_s$  we have mixing between the  $\sigma$ ,  $\sigma'$  and the neutral  $\sigma_\pi$ , the latter decoupling from the former if  $SU(2)$  isospin degeneracy,  $m_u = m_d$ , is imposed.

The same techniques applied in Secs. II B and II C can now be directly applied to the scalar resonances, with two changes: (i) one has to replace the coupling constants  $K_i^+$  of the previous section by  $K_i^-$  given in Eq. (3) and (ii) the pseudoscalar polarizations are replaced by their scalar counterparts:

$$\Pi_{q\bar{q}}^S(k_0, \vec{k}) = -\frac{N_c}{8\pi^2} [2A(m_q, \mu_q) + (4m_q^2 - k^2)B_0(\vec{k}, m_q, \mu_q, m_q, \mu_q, k_0)] \quad (44)$$

$$\Pi_{s\bar{s}}^S(k_0, \vec{k}) = -\frac{N_c}{8\pi^2} [2A(m_s, \mu_s) + (4m_s^2 - k^2)B_0(\vec{k}, m_s, \mu_s, m_s, \mu_s, k_0)] \quad (45)$$

$$\begin{aligned} \Pi_{q\bar{s}}^S(k_0, \vec{k}) = & -\frac{N_c}{8\pi^2} [A(m_q, \mu_q) + A(m_s, \mu_s) \\ & + \left( (m_q + m_s)^2 - (k_0 + \mu_q - \mu_s)^2 + \vec{k}^2 \right) B_0(\vec{k}, m_q, \mu_q, m_s, \mu_s, k_0)] \quad , \end{aligned} \quad (46)$$

which are derived from the same graph as in Fig. 2, dropping the  $i\gamma_5$  factors at the vertices.

## E. Numerical Results

For our numerical calculations, we employ the parameter set  $m_{0q} = 5.5 \text{ MeV}$ ,  $m_{0s} = 140.7 \text{ MeV}$ ,  $G\Lambda^2 = 1.835$ ,  $K\Lambda^5 = 12.36$  and  $\Lambda = 602.3 \text{ MeV}$ , that has been determined on fixing the conditions  $m_\pi = 135.0 \text{ MeV}$ ,  $m_K = 497.7 \text{ MeV}$ ,  $m_{\eta'} = 957.8 \text{ MeV}$  and  $f_\pi = 92.4 \text{ MeV}$ , while  $m_{0q}$  is fixed at 5.5 MeV. The reason why we fitted the mass of the  $\eta$  instead of the  $\eta'$  has a purely technical origin. This parameter set gives an  $\eta$  mass of  $m_\eta = 514.8 \text{ MeV}$ , which compares reasonably well with the physical value  $m_\eta = 548.8 \text{ MeV}$ . Although we have developed the general formalism to include the case of finite chemical potentials, we confine ourselves to  $\mu_q = \mu_s = 0$  in what follows.

Figure 3 shows the temperature dependence of the constituent quark masses. At  $T = 0$ , we find  $m_q = 367.7 \text{ MeV}$  and  $m_s = 549.5 \text{ MeV}$ . At temperatures around 200 MeV the mass of the light quarks drops to the current quark mass, indicating a washed out crossover from the chirally broken to approximately chirally symmetric phase. The strange quark mass starts to decrease significantly in this temperature range, but even at  $T = 300 \text{ MeV}$  it is still a factor of two away from the strange current quark mass.

Figure 4 shows the temperature dependence of the pseudoscalar meson masses at  $\mu = 0$ . For comparison, the curves of  $2m_q$  and  $m_q + m_s$  are also indicated. At low temperatures, the meson masses are approximately constant. The crossing of the  $\pi$  and  $\eta$  lines with the  $2m_q$  line indicates the respective Mott transition temperature for these particles,  $T_{M\pi}$  and  $T_{M\eta}$ . One observes that  $T_{M\eta} < T_{M\pi}$ , the absolute values are  $T_{M\eta} = 180 \text{ MeV}$  and  $T_{M\pi} = 212 \text{ MeV}$ . For temperatures higher than  $T_{M\pi}$ ,  $T_{M\eta}$ , respectively, the  $\pi$  and  $\eta$  become resonances and their masses increase. Similarly a Mott transition temperature  $T_{MK}$  for the kaon modes can be defined at the point where  $m_K$  meets  $m_s + m_q$ . This is also indicated in the figure. One can also see from this plot that  $T_{M\pi}$  and  $T_{MK}$  are approximately equal, with  $T_{MK} = 210 \text{ MeV}$ .

Figure 5 shows the absolute values of the pion and kaon coupling constants. A striking behaviour is observed at the Mott temperature. There the polarization displays a kink singularity, which can also be seen in the meson masses. Technically this results in the coupling strengths approaching zero for  $T \rightarrow T_M$  from below. This behaviour differs markedly from the behaviour of the couplings when evaluated in

the chiral limit. In that case, the coupling strength is *always* different from zero as one approaches the transition temperature from below. Note that this strong deviation from the chiral limit behaviour may have extreme consequences for results that depend strongly on this function, such as the cross sections. Since we regard the physical situation as being non-chiral, we investigate this situation only, and draw conclusions accordingly. The  $\eta$ -quark couplings have not been explicitly shown; they display a qualitatively similar behaviour.

The numerical calculations of the scalar mass spectrum are shown in Fig. 6. At  $T = 0$ , we find  $m_\sigma = 728.9$  MeV,  $m_{\sigma'} = 1198.3$  MeV,  $m_{\sigma\pi} = 880.2$  MeV and  $m_{\sigma_K} = 1050.5$  MeV. For comparison, the double constituent quark mass is also shown in the figure. All these mesons are unstable over the entire temperature range, except for the  $\sigma$ , for which the mixing results in a mass slightly below  $2m_q$  at  $T = 0$ . Although the difference is small compared to the standard two flavor model, it has the qualitative effect of making the  $\sigma$  a stable particle for temperatures up to its Mott temperature  $T_{M\sigma} = 165$  MeV. As in the two flavor model, we obtain  $m_\sigma \approx m_\pi$  above the pion Mott temperature, as is expected from symmetry requirements.

The results presented in this section compare well with those of Ref. [9].

### III. HADRONIZATION CROSS SECTIONS

#### A. Classification of Hadronization Processes

Since a large number of hadronization processes are available to the light and strange sector quarks, it is useful to introduce a classification scheme to simplify the task of bookkeeping. The cross sections are classified according to the incoming quarks and include all exit channels [12]. Since we work in the approximation  $m_u = m_d$ , we have isospin symmetry and charge conjugation, leading to the relations

$$\sigma_{u\bar{d}} = \sigma_{d\bar{u}} \tag{47a}$$

$$\sigma_{u\bar{s}} = \sigma_{d\bar{s}} = \sigma_{s\bar{u}} = \sigma_{s\bar{d}} \tag{47b}$$

$$\sigma_{u\bar{u}} = \sigma_{d\bar{d}} , \tag{47c}$$

using an obvious notation. Together with  $\sigma_{s\bar{s}}$ , we thus have four independent classes of hadronization cross sections,  $\sigma_{u\bar{d}}$ ,  $\sigma_{u\bar{s}}$ ,  $\sigma_{u\bar{u}}$  and  $\sigma_{s\bar{s}}$ . For these four classes, we determine the hadronization processes that are not forbidden by charge, strangeness or isospin conservation. These conservation laws lead to the processes that are listed in Table I.

For the outgoing channels in Table I, further symmetry relations hold:

$$\sigma_{u\bar{s} \rightarrow \pi^+ K^0} = 2\sigma_{u\bar{s} \rightarrow \pi^0 K^+} \quad (48a)$$

$$\sigma_{u\bar{d} \rightarrow \pi^+ \eta} = 2\sigma_{u\bar{u} \rightarrow \pi^0 \eta} \quad (48b)$$

$$\sigma_{u\bar{d} \rightarrow \pi^+ \eta'} = 2\sigma_{u\bar{u} \rightarrow \pi^0 \eta'} \quad (48c)$$

$$\sigma_{s\bar{s} \rightarrow K^+ K^-} = \sigma_{s\bar{s} \rightarrow K^0 \bar{K}^0} \quad (48d)$$

$$\sigma_{s\bar{s} \rightarrow \pi^+ \pi^-} = 2\sigma_{s\bar{s} \rightarrow \pi^0 \pi^0} , \quad (48e)$$

as a consequence of flavor algebra. In total, there are nineteen independent cross sections that we calculate.

## B. Feynman Graphs

The Feynman graphs that we consider, have the generic forms shown in fig. 7. This choice of diagrams is in keeping with the evaluation of the Hartree diagram to determine the gap equation and the random phase approximation for the polarization. Together this selection constitutes a consistent expansion in the inverse number of colors,  $1/N_c$  [13–15]. We stress that this is not an expansion in the coupling strength, but is rather a non-perturbative expansion. Note that the calculation of the transition amplitudes is complicated with respect to the  $SU(2)$  isospin symmetric case by the fact that here each fermion line carries a flavor dependent mass, while the meson lines in turn carry differing masses also. We therefore attempt to retain as general a formalism as possible in what follows for the transition amplitudes and we specify the parameters later.

### 1. $s$ channel

The  $s$  channel exchange diagrams have the form

$$-i\mathcal{M}_s = \bar{v}(p_2)u(p_1)\delta_{c_1c_2}f_s i\mathcal{D}(p_1 + p_2)\Gamma(p_1 + p_2; p_3)ig_1ig_2 , \quad (49)$$

where  $g_1, g_2$  are meson–quark coupling strengths for the outgoing mesons and  $f_s$  is a flavor factor. The momenta of the incoming particles are  $p_1$  and  $p_2$ . For the outgoing particles, we assign momenta  $p_3$  and  $p_4$ .  $\mathcal{D}$  stands for the scattering amplitude of the virtual scalar meson. It can either take the form appropriate for a scalar meson that corresponds to Eqs. (8, 9), if the incoming quarks have different flavor, or it can be constructed as the sum over mixing terms according to Eq. (24), in all cases with  $K_i^+$  replaced by  $K_i^-$ , and  $\Pi^P$  by  $\Pi^S$ . The symbol  $\Gamma$  describes the three meson vertex contribution to the diagram. Its general form in the imaginary time formalism is (cf. Fig. 8)

$$\begin{aligned} \Gamma(i\nu_m, \vec{k}; i\alpha_l, \vec{p}) &= -N_c \frac{i}{\beta} \sum_n \int \frac{d^3q}{(2\pi)^3} \\ &\times \text{tr}_\gamma \left[ iS^{f_1}(i\omega_n, \vec{q})i\gamma_5 iS^{f_2}(i\omega_n - i\alpha_l, \vec{q} - \vec{p})i\gamma_5 iS^{f_3}(i\omega_n - i\nu_m, \vec{q} - \vec{k}) \right] , \end{aligned} \quad (50)$$

where  $(i\nu_m, \vec{k})$  is the four momentum of the incoming scalar meson and  $(i\alpha_l, \vec{p})$  the four momentum of one of the outgoing mesons. It is once again understood that the complex meson frequencies are to be analytically continued at the end of the calculation. Taking the spinor trace in Eq. (50) leads to the form

$$\begin{aligned} \Gamma(i\nu_m, \vec{k}; i\alpha_l, \vec{p}) &= \frac{4N_c}{\beta} \sum_n \int \frac{d^3q}{(2\pi)^3} \\ &\times \frac{A - B}{[(i\omega_n + \mu_1)^2 - E_1^2][(i\omega_n - i\alpha_l + \mu_2)^2 - E_2^2][(i\omega_n - i\nu_m + \mu_3)^2 - E_3^2]} \end{aligned} \quad (51)$$

with

$$A = m_3\vec{q}(\vec{q} - \vec{p}) - m_2\vec{q}(\vec{q} - \vec{k}) + m_1(\vec{q} - \vec{p})(\vec{q} - \vec{k}) + m_1m_2m_3 \quad (52)$$

$$\begin{aligned} B &= m_3(i\omega_n + \mu_1)(i\omega_n - i\alpha_l + \mu_2) - m_2(i\omega_n + \mu_1)(i\omega_n - i\nu_m + \mu_3) \\ &\quad + m_1(i\omega_n - i\alpha_l + \mu_2)(i\omega_n - i\nu_m + \mu_3) \end{aligned} \quad (53)$$

and for which the abbreviations  $E_1 = \sqrt{\vec{q}^2 + m_1^2}$ ,  $E_2 = \sqrt{(\vec{q} - \vec{p})^2 + m_2^2}$  and  $E_3 = \sqrt{(\vec{q} - \vec{k})^2 + m_3^2}$  have been introduced.

As was done in the case of the polarization, it is useful to make a decomposition of this function in terms of elementary integrals

$$\begin{aligned} \Gamma(i\nu_m, \vec{k}; i\alpha_l, \vec{p}) = & -\frac{N_c}{8\pi^2} \left[ (m_3 - m_2)B_0(\vec{k} - \vec{p}, m_2, \mu_2, m_3, \mu_3, i\nu_m - i\alpha_l) \right. \\ & + (m_1 - m_2)B_0(\vec{p}, m_1, \mu_1, m_2, \mu_2, i\alpha_l) \\ & + (m_1 + m_3)B_0(\vec{k}, m_1, \mu_1, m_3, \mu_3, i\nu_m) \\ & + \left[ m_1^2(m_3 - m_2) + m_2^2(m_1 + m_3) + m_3^2(m_1 - m_2) - 2m_1m_2m_3 \right. \\ & + m_3(\vec{p}^2 - (i\alpha_l - \mu_2 + \mu_1)^2) - m_2(\vec{k}^2 - (i\nu_m - \mu_3 + \mu_1)^2) \\ & \left. \left. + m_1((\vec{p} - \vec{k})^2 - (i\alpha_l - i\nu_m - \mu_2 + \mu_3)^2) \right] \right. \\ & \left. \times C_0(\vec{p}, \vec{k}, m_1, \mu_1, m_2, \mu_2, i\alpha_l, m_3, \mu_3, i\nu_m) \right] . \end{aligned} \quad (54)$$

The function  $B_0$  has already been given in Eq. (12). It is necessary to introduce a third loop integral  $C_0$  (cf. Appendix A), which is explicitly given as

$$\begin{aligned} C_0(\vec{p}, \vec{k}, m_1, \mu_1, m_2, \mu_2, i\alpha_l, m_3, \mu_3, i\nu_m) = & \frac{16\pi^2}{\beta} \sum_n e^{i\omega_n \eta} \int_{|\vec{p}| < \Lambda} \frac{d^3 q}{(2\pi)^3} \\ & \times \frac{1}{((i\omega_n + \mu_1)^2 - E_1^2)} \frac{1}{((i\omega_n - i\alpha_l + \mu_2)^2 - E_2^2)} \frac{1}{((i\omega_n - i\nu_m + \mu_3)^2 - E_3^2)} . \end{aligned} \quad (55)$$

As with the polarization function that was given in Eq. (11), Eqs. (50–54) are defined intentionally without any flavor factors.

## 2. *t* and *u* channels

The *t* and *u* channel exchange diagrams shown in Fig. 7 have the general form

$$\begin{aligned} -i\mathcal{M}_t = & f_t \delta_{c_1 c_2} \bar{v}(p_2) i\gamma_5(i g_1) \frac{i}{\not{p}_1 - \not{p}_3 - m^{(t)}} i\gamma_5(i g_2) u(p_1) \\ = & i \frac{g_1 g_2 f_t}{t - m^{(t)2}} \delta_{c_1 c_2} \bar{v}(p_2) \gamma_5(\not{p}_1 - \not{p}_3 + m^{(t)}) \gamma_5 u(p_1) \end{aligned} \quad (56)$$

$$-i\mathcal{M}_u = i \frac{g_1 g_2 f_u}{u - m^{(u)2}} \delta_{c_1 c_2} \bar{v}(p_2) \gamma_5(\not{p}_1 - \not{p}_4 + m^{(u)}) \gamma_5 u(p_1) \quad (57)$$

where, once again  $g_1, g_2$  are the quark–meson couplings for the outgoing mesons, and  $f_t, f_u$  account for flavor factors from the Gell–Mann matrices. The momenta of

the incoming quark and antiquark are  $p_1$  and  $p_2$ , those of the outgoing mesons  $p_3$  and  $p_4$ . The mass of the exchanged fermion is denoted by  $m^{(t)}$  and  $m^{(u)}$  respectively. Note that these masses are not necessarily equal.

For any actual calculation of cross sections and transition rates, one needs to sum the relevant amplitudes, take the absolute value squared and to sum over final and to average over initial states. Our results are listed in Appendix B.

### C. Calculation of Cross Sections

Having provided the prerequisites for calculation, we illustrate the main features via examples. (i) The process  $u\bar{d} \rightarrow \pi^+\pi^0$  provides an example in which a  $u$  channel diagram is required. Such a diagram occurs not only when the outgoing mesons are identical. (ii) The process  $u\bar{s} \rightarrow \pi^+K^0$  is chosen because it has unequal masses for the incoming quarks, the virtual quarks of the vertex part, and the outgoing mesons. (iii) The process  $u\bar{u} \rightarrow \pi^+\pi^-$  demonstrates the usage of mixing propagators for the virtual scalar mesons in the  $s$  channel. Together, these three examples indicate how the calculation is performed in general.

We assume that the centre of mass system of the incoming quarks is at rest relative to the medium. All quantities, such as couplings  $g_{\pi q\bar{q}}$ , are calculated within this framework, and this is used in all processes calculated, e. g. in triangle diagrams. Since this implies that  $\vec{k} = \vec{0}$  in Eqs. (50)–(55), the vertex function  $\Gamma$  then depends only on the absolute value of the meson momentum. This leads to the fact that the total cross section depends only on the invariant energy  $s$  and the temperature  $T$  [12].

In what follows, we drop the momentum arguments of the scalar meson propagator  $\mathcal{D}$  and the three meson vertex  $\Gamma$  for simplicity.

#### 1. Calculation of $\sigma_{u\bar{d} \rightarrow \pi^+\pi^0}$

Explicit graphs for this process are shown in Fig. 9. We have two graphs of the  $s$  channel type, which we label  $s$  and  $s'$ , respectively. The flavor factors for these graphs are found to be

$$f_s = -f_{s'} = -2\sqrt{2} \quad (58a)$$

$$f_t = -f_u = -\sqrt{2} \quad . \quad (58b)$$

The relative sign of  $f_s$ ,  $f_{s'}$  and  $f_t$ ,  $f_u$  arises from the flavor matrix  $\lambda_3$  that occurs at the  $\pi^0$  vertex, whose  $uu$  and  $dd$  components have opposite sign.

The virtual meson exchanged in this case is a charged  $\sigma_\pi$ , so that one may identify

$$\mathcal{D}_s = \mathcal{D}_{s'} = \frac{2K_1^-}{1 - 4K_1^- \Pi_{q\bar{q}}^S(\sqrt{s}, \vec{0})} \quad . \quad (59)$$

The contribution of the vertex graph in the centre of mass system turns out in this case to be the same for both  $s$  channel type graphs. From our general formula Eq. (54), one has

$$\begin{aligned} \Gamma_s = \Gamma_{s'} = -\frac{N_c m_q}{8\pi^2} & \left[ 2B_0(\vec{0}, m_q, \mu_q, m_q, \mu_q, \sqrt{s}) \right. \\ & \left. + (s - 2m_\pi^2)C_0(\vec{p}_3, \vec{0}, m_q, \mu_q, m_q, \mu_q, \frac{1}{2}\sqrt{s}, m_q, \mu_q, \sqrt{s}) \right] \quad , \end{aligned} \quad (60)$$

where  $|\vec{p}_3| = \frac{1}{2}\sqrt{s - 4m_\pi^2}$  is the momentum of the outgoing  $\pi^+$ . The total contribution of the  $s$  channel type graphs is thus

$$\begin{aligned} -i(\mathcal{M}_s + \mathcal{M}_{s'}) &= -i\bar{v}(p_2)u(p_1)\delta_{c_1c_2}g_{\pi q\bar{q}}^2(f_s\mathcal{D}_s\Gamma_s + f_{s'}\mathcal{D}_{s'}\Gamma_{s'}) \\ &= 0 \quad , \end{aligned} \quad (61)$$

which resembles the result for the two flavor model [12], where this process has no  $s$  channel due to the lack of charged scalar resonances.

The squared invariant amplitude thus arises from the  $t$  and  $u$  channels alone. From Eqs. (B2), (B3) and (B6), this takes the form

$$\begin{aligned} \frac{1}{4N_c^2} \sum_{s,c} |\mathcal{M}_t + \mathcal{M}_u|^2 &= \frac{|g_{\pi q\bar{q}}|^4}{N_c} \left[ \frac{s(m_q^2 - t) - (t - m_\pi^2 - m_q^2)^2}{(t - m_q^2)^2} \right. \\ &+ \frac{s(m_q^2 - u) - (u - m_\pi^2 - m_q^2)^2}{(u - m_q^2)^2} \\ & \left. - 2\frac{(t - m_\pi^2 - m_q^2)(m_\pi^2 + m_q^2 - u) + sm_\pi^2}{(t - m_q^2)(u - m_q^2)} \right] \quad . \end{aligned} \quad (62)$$

In the limit  $m_\pi \rightarrow 0$ , this reduces to an extremely simple expression. This differs from that given in Ref. [12], in which the  $u$  channel has been omitted.

We obtain the differential cross section for this process to be

$$\frac{d\sigma_{u\bar{d}\rightarrow\pi^+\pi^0}}{dt} = \frac{1}{16\pi s(s-4m_q^2)} \frac{1}{4N_c^2} \sum_{s,c} |\mathcal{M}_t + \mathcal{M}_u|^2 \quad . \quad (63)$$

The total cross section is now constructed from the integration over the exchanged momentum  $t$  as [12]

$$\sigma_{u\bar{d}\rightarrow\pi^+\pi^0}(s, T) = \int dt \frac{d\sigma_{u\bar{d}\rightarrow\pi^+\pi^0}}{dt} (1 + f_B(\frac{1}{2}\sqrt{s}))^2 \quad . \quad (64)$$

The Bose distribution function  $f_B(x) = 1/(\exp(\beta x) - 1)$  is introduced, since the presence of mesons in the heat bath leads to an enhancement of the meson creation process in the medium.

## 2. Calculation of $\sigma_{u\bar{s}\rightarrow\pi^+K^0}$

The Feynman graphs for this process are shown in Fig. 10. Here only one  $s$  channel diagram is possible. From the graphs, we find the flavor factors

$$f_s = 4 \quad (65a)$$

$$f_t = 2 \quad . \quad (65b)$$

The virtual scalar meson exchanged in the  $s$  channel is a  $\sigma_K$ , so that we have

$$\mathcal{D} = \frac{2K_4^-}{1 - 4K_4^- \Pi_{q\bar{s}}^S(\sqrt{s}, \vec{0})} \quad . \quad (66)$$

The contribution of the vertex part can be derived from our general formula Eq. (54) to be

$$\begin{aligned} \Gamma = & -\frac{N_c}{8\pi^2} \left[ (m_s - m_q) B_0(\vec{p}_4, m_q, \mu_q, m_s, \mu_s, E_4) \right. \\ & + (m_s + m_q) B_0(\vec{0}, m_q, \mu_q, m_s, \mu_s, \sqrt{s}) \\ & - \left[ m_s m_\pi^2 + m_q (m_K^2 - s + 2E_3(\mu_s - \mu_q)) \right] \\ & \left. \times C_0(\vec{p}_3, \vec{0}, m_q, \mu_q, m_q, \mu_q, E_3, m_s, \mu_s, \sqrt{s}) \right] \quad , \quad (67) \end{aligned}$$

where  $(E_3, \vec{p}_3)$  and  $(E_4, \vec{p}_4)$  denote the four momenta of the  $\pi^+$  and the  $K^0$ , respectively. Because the masses of the outgoing particles are different, the momentum of the  $\pi^+$  say, now has to be determined via

$$|\vec{p}_3| = \frac{1}{2\sqrt{s}} \sqrt{(s - (m_\pi + m_K)^2)(s - (m_\pi - m_K)^2)} \quad . \quad (68)$$

From the formulae in Appendix B, one obtains the squared transition amplitude as

$$\begin{aligned} \frac{1}{4N_c^2} \sum_{s,c} |\mathcal{M}_s + \mathcal{M}_t|^2 = & \frac{8|g_{\pi q\bar{q}}g_{Kq\bar{s}}|^2}{N_c} \left( |\mathcal{D}\Gamma|^2 (s - (m_q + m_s)^2) \right. \\ & - \frac{\Re(\mathcal{D}\Gamma)}{t - m_q^2} \left( m_q(s - m_K^2 + m_\pi^2) \right. \\ & \left. \left. + (t - m_q^2 - m_\pi^2)(m_q + m_s) \right) \right. \\ & + \frac{1}{4(t - m_q^2)^2} \left( (m_\pi^2 + m_q^2 - t)(t - m_K^2 + m_s^2) \right. \\ & \left. \left. + (m_q^2 - t)(s - m_q^2 - m_s^2) - 2m_s m_q m_\pi^2 \right) \right) \quad , \end{aligned} \quad (69)$$

with  $\Re$  denoting the real part of the function following.

Due to the different masses of the  $u$  and  $s$  quarks, the differential cross section is now given as

$$\frac{d\sigma_{u\bar{s} \rightarrow \pi^+ K^0}}{dt} = \frac{1}{64\pi s \vec{p}_1^2} \frac{1}{4N_c^2} \sum_{s,c} |\mathcal{M}_s + \mathcal{M}_t|^2 \quad . \quad (70)$$

Again, the momentum  $|\vec{p}_1|$  has to be calculated using Eq. (68), where  $m_\pi$ ,  $m_K$  have to be replaced by  $m_q$ ,  $m_s$ , respectively.

The total cross section is defined to be

$$\sigma_{u\bar{s} \rightarrow \pi^+ K^0}(s, T) = \int dt \frac{d\sigma_{u\bar{s} \rightarrow \pi^+ K^0}}{dt} (1 + f_B(E_3))(1 + f_B(E_4)) \quad (71)$$

in this case.

### 3. Calculation of $\sigma_{u\bar{u} \rightarrow \pi^+ \pi^-}$

The Feynman graphs for this process are shown in Fig. 11. Once again, we have  $s$  and  $s'$  channel graphs. Since the incoming quarks have the same flavor, we have to consider mixing for the virtual mesons. The propagator for the  $s$  graph reads

$$\mathcal{D}_s = M_{\sigma_\pi} + \frac{1}{3} (2M_{00} + 2\sqrt{2}M_{08} + M_{88}) \quad , \quad (72)$$

while the propagator for the  $s'$  graph is

$$\mathcal{D}_{s'} = -M_{\sigma\pi} + \frac{1}{3} (2M_{00} + 2\sqrt{2}M_{08} + M_{88}) \quad . \quad (73)$$

Here the flavor factors for the virtual meson vertices have already been taken into account, so that we only have to consider the flavor factors from the outgoing mesons, which contribute a factor  $\sqrt{2}$  at every vertex:

$$f_s = f_{s'} = f_t = 2 \quad . \quad (74)$$

The meson vertex part of the  $s$  and  $s'$  graph is the same as for  $u\bar{d} \rightarrow \pi^+\pi^0$ , as was given in Eq. (60). Since we need the sum  $\mathcal{M}_s + \mathcal{M}_{s'}$ , we find that the contribution of the  $\sigma_\pi$  in this combination cancels and we obtain

$$-i(\mathcal{M}_s + \mathcal{M}_{s'}) = -i\bar{v}(p_2)u(p_1)\delta_{c_1c_2}g_{\pi q\bar{q}}^2 \frac{4}{3} (2M_{00} + 2\sqrt{2}M_{08} + M_{88}) \Gamma \quad . \quad (75)$$

The rest of the calculation proceeds as in the previous two cases discussed.

#### IV. NUMERICAL RESULTS

In this section, we present our numerical results. Since we are interested in the cross sections as an input to transport equations, we choose to give the transition rates  $w(s, T)$  instead of the integrated cross sections  $\sigma(s, T)$ . These two quantities are related by [18]

$$w(s, T) = |\vec{v}_{\text{rel}}| \sigma(s, T) \quad , \quad (76)$$

where the relative velocity of the incoming particles in the centre of mass system is

$$|\vec{v}_{\text{rel}}| = \frac{\sqrt{(p_1 p_2)^2 - (m_1 m_2)^2}}{E_1 E_2} \quad . \quad (77)$$

For equal masses of the incoming quarks,  $m_1 = m_2 = m$ , this can be expressed in terms of the centre of mass energy  $s$  as

$$|v_{\text{rel}}| = 2\sqrt{1 - \frac{4m^2}{s}} \quad . \quad (78)$$

The introduction of the transition rate as opposed to the cross sections has a further advantage in that it suppresses the kinematic singularity which appears at the threshold for the exothermic reactions  $q\bar{q} \rightarrow M_1 M_2$  where  $2m_q > m_{M_1} + m_{M_2}$ .

To commence, we choose to discuss one simple process, and decompose the calculation into its constituent  $s$ ,  $t$  and  $u$  channel graphs, in order to indicate the relative magnitude of these contributions. We pick the process  $u\bar{d} \rightarrow \pi^+\eta$ , that by Eq. (48b) can also be regarded as a component of the  $\sigma_{u\bar{u}}$  calculation. The appropriate Feynman diagrams can be obtained from Fig. 9 on replacing the  $\pi^0$  by  $\eta$  in this figure. There are two  $s$  channel, one  $t$  channel and one  $u$  channel exchanges possible. In this case, we find  $f_s = f_{s'}$  and  $f_t = f_u$ , so the  $s$  channels do not cancel. We display these contributions explicitly in Fig. 12. Here we plot the transition rate that originates from  $|\mathcal{M}_t|^2$  (which is equal to the contribution from  $|\mathcal{M}_u|^2$ ),  $|\mathcal{M}_s|^2$ ,  $|\mathcal{M}_{s'}|^2$ , the sum  $|\mathcal{M}_t + \mathcal{M}_u|^2$ , and the sum of all four graphs,  $|\mathcal{M}_s + \mathcal{M}_{s'} + \mathcal{M}_t + \mathcal{M}_u|^2$ . From this figure, one can see that the  $t$  and  $u$  channels give the dominant contributions. Although the velocity factor in Eq. (76) goes to zero at threshold, the  $t$  channel contribution stays finite. However, it cancels against the  $u$  channel contribution, thus yielding a zero total rate here. This is a rather general feature that we wish to point out. Such a cancellation occurs for all processes where the flavor factors of the  $t$  and  $u$  channel graphs are equal,  $f_t = f_u$ . We notice also that the  $s$  channel contributions are comparatively small, except in the region  $\sqrt{s} \approx 0.5\text{--}1\text{ GeV}$ , where they exhibit a resonance structure due to the  $\sigma_\pi$  exchange. At threshold, their contributions go to zero, since they are proportional to  $s - 4m_q^2$ , as can be seen explicitly from Eq. (B1). This demonstrates the generic features that are empirically observed in all of our calculations: in general the  $t$  and  $u$  channels dominate, while the  $s$  channel only plays a role over a small region if a resonance is excited.

We turn now to a discussion of the four possible hadronization rates, that stem from the four independent cross section classes  $\sigma_{u\bar{d}}$ ,  $\sigma_{u\bar{s}}$ ,  $\sigma_{u\bar{u}}$  and  $\sigma_{s\bar{s}}$  that were listed in Table I.

#### A. $u\bar{d} \rightarrow \text{hadrons}$

Figure 13 shows the hadronization rate of  $u\bar{d} \rightarrow \text{hadrons}$  at  $T = 0$  as a function of  $\sqrt{s}$ . Here we have shown the contributions from individual processes, in this case being  $u\bar{d} \rightarrow \pi^+\pi^0$ ,  $K^+\overline{K^0}$  and  $\pi^+\eta$ . The contribution from the process  $u\bar{d} \rightarrow \pi^+\eta'$  is negligible and has thus not been shown. One recognizes from this figure that the transition rate is dominated by the process  $u\bar{d} \rightarrow \pi^+\pi^0$ , as is expected physically. A

further physical feature that is common to all the calculations is also illustrated here, and we thus comment at this point: that is, that an *exothermic* process displays a finite rate at threshold. An exception to this rule follows for processes such as  $u\bar{d} \rightarrow \pi^+\eta$  (which are also exothermic), where equal flavor factors occur in both the  $t$  and  $u$  channel exchanges and the amplitudes cancel, as was discussed above. By contrast, the process  $u\bar{d} \rightarrow K^+\overline{K^0}$  is *endothermic*, which means that the threshold shifts from  $\sqrt{s} = 2m_q$  to  $\sqrt{s} = 2m_K$ , where it yields a zero rate. Finally we comment that the relative magnitude of the three rates contributing to the total rate essentially reflects the available phase space.

In Fig. 14, we show the hadronization rate at various values of the temperature,  $T = 0$ ,  $T = 150$  MeV,  $T = 190$  MeV and  $T = 250$  MeV as a function of  $\sqrt{s}$ . The threshold value of  $\sqrt{s}$  at which hadronization sets in is different for the four cases due to the temperature dependence of the quark and meson masses. At  $T = 0$  and  $T = 150$  MeV the dominant process,  $u\bar{d} \rightarrow \pi^+\pi^0$ , is exothermic, thus giving rise to a finite rate at the threshold  $\sqrt{s} = 2m_q$ . At  $T = 190$  MeV and  $T = 250$  MeV on the other hand, the pions are more massive than the quarks, so that this process becomes endothermic and the threshold is given in this case as  $\sqrt{s} = 2m_\pi$ . Thus the finite values at thresholds observed in the rates at lower temperatures change to become maxima slightly above threshold, and a zero rate is obtained at these thresholds.

In Fig. 15, we show an example for the differential cross section  $d\sigma/d\cos\theta$  at zero temperature and at  $\sqrt{s} = 1.5$  GeV. Again the contribution of  $u\bar{d} \rightarrow \pi^+\eta'$  is negligible and is thus not shown. One notices a forward–backward asymmetry in this plot, which is solely due to kaon production. Physically one can understand this as follows: after the reaction  $u\bar{d} \rightarrow K^+\overline{K^0}$  has occurred, the incoming  $u$  quark has become a constituent of the  $K^+$ , so that the produced  $K^+$  preferentially takes the direction of the incoming  $u$ . In the other reactions,  $u\bar{d} \rightarrow \pi^+\pi^0$ ,  $\pi^+\eta$  and  $\pi^+\eta'$  however, the  $u$  can become a constituent of any one of the produced particles, which makes these reactions forward–backward symmetric.

### B. $u\bar{s} \rightarrow$ hadrons

Figure 16 gives the transition rate for  $u\bar{s} \rightarrow$  hadrons at  $T = 0$  as a function of  $\sqrt{s}$ , decomposed into its constituent processes. The dominant contributions to the transition rate come from the processes  $u\bar{s} \rightarrow \pi^+ K^0$  and  $u\bar{s} \rightarrow \pi^0 K^+$ , which give the same up to a factor of two. We again note that these are exothermic processes, thus leading to a finite transition rate at the threshold  $\sqrt{s} = m_q + m_s$ . For  $\sqrt{s}$  slightly above threshold, a maximum appears in the transition rate of  $u\bar{s} \rightarrow \pi^+ K^0$ ,  $\pi^0 K^+$ , that corresponds to an excitation of the  $\sigma_K$  resonance. This maximum is not visible in the overall summed rate at this temperature, since it is dominated rather by  $u\bar{s} \rightarrow K^+ \eta$  production.

Figure 17 shows the transition rates at the temperatures  $T = 0$ ,  $T = 150$  MeV,  $T = 190$  MeV,  $T = 250$  MeV as a function of  $\sqrt{s}$ . The  $\sigma_K$  excitation, that is not visible at  $T = 0$ , is now clearly seen at  $T = 150$  MeV and  $T = 190$  MeV. At  $T = 0$  and  $T = 150$  MeV, the threshold is determined as  $\sqrt{s} = m_q + m_s$ , and the reaction is exothermic, while for  $T = 190$  MeV and  $T = 250$  MeV, the reactions are endothermic, with threshold value  $\sqrt{s} = m_\pi + m_K$ . Correspondingly, in the exothermic regime, the transition rate is finite at threshold, while at higher temperatures, where the outgoing mesons have become more massive than the incoming quark and antiquark, the transition rate vanishes at the threshold value.

### C. $u\bar{u} \rightarrow$ hadrons

The contributions of the various processes for  $u\bar{u} \rightarrow$  hadrons at  $T = 0$  are shown in Fig. 18 as a function of  $\sqrt{s}$ . Here we plot only the transition rates for the production of  $\pi^+ \pi^-$ ,  $\pi^0 \pi^0$ ,  $K^+ K^-$  and  $\pi^0 \eta$ . All other channels are negligible. One notices that the transition rate is dominated by  $\pi^+ \pi^-$  production. For  $\sqrt{s} > 1$  GeV, the  $K^+ K^-$  production appears to be the next most important process, followed by  $\pi^0 \pi^0$  and  $\pi^0 \eta$ . We observe that the contribution of  $u\bar{u} \rightarrow \pi^0 \pi^0$  is rather small in comparison with  $u\bar{u} \rightarrow \pi^+ \pi^-$ . We can trace this back to the allowed Feynman diagrams and the associated flavor algebra. It turns out that the  $s$  channel exchanges for both processes give the same contribution in total, although they have differing flavor factors associated with them. On the other hand, the  $t$  channel exchange for  $\pi^0 \pi^0$  contributes one half that obtained for  $\pi^+ \pi^-$  hadronization, due to the

associated flavor factors ( $f_t = 1$  for  $u\bar{u} \rightarrow \pi^0\pi^0$ ,  $f_t = 2$  for  $u\bar{u} \rightarrow \pi^+\pi^-$ ). In addition, the  $u\bar{u} \rightarrow \pi^0\pi^0$  also has an  $u$  channel exchange available. This tends to cancel the  $t$  channel exchange. Finally, the  $t$  integration runs only over half of the available phase space for the process  $u\bar{u} \rightarrow \pi^0\pi^0$  [12]. These features result in a considerable reduction in the production of  $\pi^0\pi^0$  over  $\pi^+\pi^-$ . We also point out that the production of  $K^0\overline{K^0}$  is negligible in contrast to the production of  $K^+K^-$ . This is due to the fact that  $u\bar{u} \rightarrow K^0\overline{K^0}$  proceeds only via a  $s$  channel graph, which gives small contributions compared to the  $t$  and  $u$  channels, as has already been discussed.

This is a direct simulation of the Zweig rule in the NJL model.

One final comment to the structures observed in Fig. 18 is with regard to the cusp seen at threshold. This is due to the excitation of the  $\sigma$  mode with  $m_\sigma \approx 2m_q$ . At  $\sqrt{s} \approx 1.2$  GeV, one notices a very weak second maximum: this comes from the  $\sigma'$ , appearing in the processes  $u\bar{u} \rightarrow K^+K^-$  and  $u\bar{u} \rightarrow K^0\overline{K^0}$ .

Figure 19 gives the rate for  $u\bar{u} \rightarrow$  hadrons at  $T = 0$ ,  $T = 150$  MeV,  $T = 190$  MeV and  $T = 250$  MeV as a function of  $\sqrt{s}$ . The cusp at the threshold value of  $\sqrt{s}$  at  $T = 0$  and  $T = 150$  MeV develops to become a sharply pronounced peak. This is a reflection of the exothermic nature of the lower temperature processes, which have threshold  $\sqrt{s} = 2m_q$ , as opposed to the endothermic processes, with threshold  $\sqrt{s} = 2m_\pi$ . In this figure, one can see the  $\sigma$  and  $\sigma'$  maxima and the shifting of the threshold due to the temperature dependence of the masses.

#### D. $s\bar{s} \rightarrow$ hadrons

Finally we show the results for  $s\bar{s} \rightarrow$  hadrons for different temperatures as a function of  $\sqrt{s}$  in Figs. 20 and 21. Here the dominant contribution comes from the processes  $s\bar{s} \rightarrow K^0\overline{K^0}$  and  $s\bar{s} \rightarrow K^+K^-$ , which have identical cross sections, and  $s\bar{s} \rightarrow \eta\eta$ . The pion production rate is very small, since these processes do not have  $t$  and  $u$  channels available, again simulating their suppression by the Zweig rule. One notices a sharp resonance in these curves near threshold. This is due to the  $\sigma'$  intermediate state. The threshold values of  $\sqrt{s}$  are determined at  $T = 0$  and  $T = 150$  MeV by  $\sqrt{s} = 2m_s$ , where the reaction is exothermic. At  $T = 190$  MeV and  $T = 250$  MeV, this is rather given by  $\sqrt{s} = 2m_K$ , since the reaction is endothermic.

## E. Averaged Transition Rates and Hadronization Times

In order to make a connection with transport theory, we introduce the energy averaged transition rate [18]

$$\bar{w}(T) = \frac{1}{\rho_1(T)\rho_2(T)} \int \frac{d^3p_1}{(2\pi)^3} \frac{d^3p_2}{(2\pi)^3} [2N_c f_F(E_1)] [2N_c f_F(E_2)] w(s, T) \quad , \quad (79)$$

which is the average transition rate for quarks and antiquarks coming from a thermal medium, their distribution being given by the Fermi function  $f_F(x) = 1/(\exp(\beta x) + 1)$ . The quark density is given as an integral over this function

$$\rho_i(T) = \int \frac{d^3p}{(2\pi)^3} 2N_c f_F \left( \sqrt{\vec{p}^2 + m_i^2} \right) \quad (80)$$

for a given quark species. In Eqs. (79, 80), the factor  $2N_c$  accounts for the number of degrees of freedom. To perform the integration, we have made the approximation that  $\sigma(s, T)$  depends only on  $s$ , even when we are not in the centre of mass system. With this assumption,  $\bar{w}(T)$  can be cast into the form

$$\bar{w}(T) = \int_{(m_1+m_2)^2}^{\infty} ds \sqrt{(p_1 p_2)^2 - (m_1 m_2)^2} \sigma(s, T) P(s, T) \quad , \quad (81)$$

where the weight function  $P(s, T)$  is given as

$$P(s, T) = \frac{1}{\rho_1(T)\rho_2(T)} \frac{1}{8\pi^4} \int_{m_1}^{\infty} dE_1 [2N_c f_F(E_1)] \times \int_{m_2}^{\infty} dE_2 [2N_c f_F(E_2)] \Theta(4|\vec{p}_1|^2|\vec{p}_2|^2 - (s - (m_1^2 + m_2^2) - 2E_1 E_2)^2) \quad . \quad (82)$$

We show the results of the average rate  $\bar{w}(T)$  for the four hadronization classes  $u\bar{d}$ ,  $u\bar{s}$ ,  $u\bar{u}$  and  $s\bar{s}$  as a function of temperature in Fig. 22. One observes that the quantity  $\bar{w}(T)$  stays fairly constant in the region from  $T \approx 50$  MeV up to the pion Mott temperature  $T_{M\pi}$ . At  $T_{M\pi}$ , it displays a minimum. This behavior differs strikingly from the curves shown in Ref. [12]: whereas the cross sections shown there decrease towards the critical temperature and then *diverge* sharply, we obtain a *minimum* at the pion Mott temperature with no divergence at all. There are two reasons for this behaviour: (i) The reason for the occurrence of the divergence has been explained in Ref. [12] as originating from the term  $d\sigma/dt \sim 1/(t - m_q^2)$  that arises from the  $t$  channel amplitude. These authors have worked in the chiral limit, so that at the critical temperature  $m_q = 0$ , and the  $t$  integration required

for the total cross section, yields a logarithmic divergence. Here, on the other hand we consider the physical situation of *finite* current quark masses, so that the quark propagators stay finite for all temperatures, and no divergence may occur. (ii) The behaviour of the cross sections is also determined by the quark–meson couplings, that multiply the transition amplitude squared. In the chiral limit, as calculated in Ref. [12], these tend to a constant value at the transition temperature, so that the overall behavior is given by the mechanism described in (i). On the other hand, in our case, when  $m_0 \neq 0$ , the quark–meson couplings strictly approach zero at the Mott temperatures, and are thus responsible for the observed behavior.

The little dip observed in the curves at  $T = 180$  MeV corresponds to the Mott temperature of the  $\eta$ ,  $T_{M\eta}$ . One also notes a discontinuity in the production rate for the class  $u\bar{u} \rightarrow$  hadrons at  $T = 165$  MeV. This occurs in the model since the  $\sigma$  in the  $SU(3) \times SU(3)$  case is weakly *bound* at  $T = 0$ , and becomes a resonance at the Mott temperature  $T_{M\sigma} = 165$  MeV. This leads to a transition rate  $\sim 1/\sqrt{s - 4m_q^2}$  and thus to a discontinuous averaged transition rate. Due to kinematic reasons, this is only visible in the processes  $u\bar{u} \rightarrow \pi^+\pi^-$  and  $u\bar{u} \rightarrow \pi^0\pi^0$  that contribute to  $u\bar{u} \rightarrow$  hadrons. Note that this structure would not appear for the  $SU(2) \times SU(2)$  NJL model, where the  $\sigma$  is a resonant state for all temperatures. This is thus a model dependent feature.

From  $\bar{w}(T)$  we compute the hadronization times

$$\tau_u^{-1}(T) = \bar{w}_{u\bar{u}}(T)\rho_{\bar{u}} + \bar{w}_{u\bar{d}}(T)\rho_{\bar{d}} + \bar{w}_{u\bar{s}}(T)\rho_{\bar{s}} \quad (83)$$

$$\tau_s^{-1}(T) = \bar{w}_{s\bar{u}}(T)\rho_{\bar{u}} + \bar{w}_{s\bar{d}}(T)\rho_{\bar{d}} + \bar{w}_{s\bar{s}}(T)\rho_{\bar{s}} . \quad (84)$$

The quantity  $\tau_u(T)$  represents the mean lifetime of a  $u$  quark in a plasma before it hadronizes into a meson. Analogously  $\tau_s(T)$  is the mean lifetime of a  $s$  quark. The numerical results are shown in Fig. 23. In the temperature region of interest,  $150 \text{ MeV} \leq T \leq 250 \text{ MeV}$ , the hadronization times are  $2\text{--}3 \text{ fm}/c$  for a  $u$  (or  $d$ ) quark, and  $3\text{--}4 \text{ fm}/c$  for a  $s$  quark. As expected, the hadronization time becomes infinite at the Mott temperature, since all hadronization cross sections go to zero here.

## F. Strangeness Production

In this section, we discuss the production rates for the processes that change the total number of  $s$  plus  $\bar{s}$  quarks. The enhancement of this quantity observed in the  $K/\pi$  ratio in nucleus–nucleus collisions over  $N+N$  collisions is one of the observables which indicates new physics [1,19,20]. The processes of interest are (i)  $u\bar{d} \rightarrow K^+ \bar{K}^0$ , (ii)  $u\bar{u} \rightarrow K^+ K^-$ ,  $K^0 \bar{K}^0$  and (iii)  $s\bar{s} \rightarrow \pi^+ \pi^-$ ,  $\pi^0 \pi^0$ ,  $\eta\eta$ ,  $\eta\eta'$ ,  $\eta'\eta'$ . While the first two reactions *increase* the total number of  $s + \bar{s}$ , the third one *decreases* this number. The production/reduction rates  $\bar{w}(T)$  are shown in Fig. 24, respectively as a function of temperature. Both increasing and decreasing processes show qualitatively the same behavior. The strangeness increasing processes are endothermic and thus occur preferentially at higher temperatures, whereas the strangeness decreasing processes (at least the dominant ones) are exothermic and thus can also happen at low temperatures. Since the processes in these three cases do not dominate their respective hadronization class, the overall magnitude of the rates is rather small compared to that shown in Fig. 22.

It is useful to define the ratio

$$\frac{(\Delta K)_{\text{gain}}}{\pi} = \frac{\bar{w}_{u\bar{d} \rightarrow K^+ K^-} + \bar{w}_{u\bar{u} \rightarrow K^+ K^-} + \bar{w}_{u\bar{u} \rightarrow K^0 \bar{K}^0}}{\bar{w}_{u\bar{d} \rightarrow \pi^+ \pi^0} + 2\bar{w}_{u\bar{d} \rightarrow \pi^+ \eta} + \bar{w}_{u\bar{u} \rightarrow \pi^+ \pi^-} + \bar{w}_{u\bar{u} \rightarrow \pi^0 \pi^0} + 2\bar{w}_{u\bar{u} \rightarrow \pi^0 \eta} + 3\bar{w}_{u\bar{u} \rightarrow \eta\eta}} \quad (85)$$

measuring the total hadronization from up and down quarks into kaons relative to the pion production due to hadronization. Here we have assumed that the  $\eta$  decays into three pions and we have neglected the contribution of the  $\eta'$ . The temperature dependence of this quantity is depicted in Fig. 25. The discontinuity at  $T = 165$  MeV is due to pion production, as has been discussed previously. Kinks occur at the respective Mott temperatures  $T_{M\sigma}$ ,  $T_{M\eta}$ ,  $T_{MK}$  and  $T_{M\pi}$ . Numerically at  $T = 150$  MeV, the strangeness enhancement ratio rises to  $(\Delta K)_{\text{gain}}/\pi = 0.01$ . This enhancement of about 1% is to be compared with the enhancement of 9% for  $S+S$  collisions at 200 GeV/A over  $N+N$  collisions, as found by the NA35 collaboration [16]. The loss term, defined as

$$\frac{(\Delta K)_{\text{loss}}}{\pi} = \frac{\rho_s \rho_{\bar{s}} (\bar{w}_{s\bar{s} \rightarrow \pi^+ \pi^-} + \bar{w}_{s\bar{s} \rightarrow \pi^0 \pi^0} + \bar{w}_{s\bar{s} \rightarrow \eta\eta'} + \bar{w}_{s\bar{s} \rightarrow \eta\eta} + \bar{w}_{s\bar{s} \rightarrow \eta'\eta'})}{2\rho_u \rho_{\bar{u}} (\bar{w}_{u\bar{d} \rightarrow \pi^+ \pi^0} + 2\bar{w}_{u\bar{d} \rightarrow \pi^+ \eta} + \bar{w}_{u\bar{u} \rightarrow \pi^+ \pi^-} + \bar{w}_{u\bar{u} \rightarrow \pi^0 \pi^0} + 2\bar{w}_{u\bar{u} \rightarrow \pi^0 \eta} + 3\bar{w}_{u\bar{u} \rightarrow \eta\eta})} \quad (86)$$

is also indicated in Fig. 25. The maximal loss is an order of magnitude less than the gain in strangeness due to hadronization. Note that the back reaction  $s\bar{s} \rightarrow$  nonstrange hadrons has been calculated under the assumption of thermal equilibrium values for  $\rho_s$  and  $\rho_{\bar{s}}$ . Should thermal equilibrium for strange quarks however not be reached, one would expect this loss term to be even more strongly suppressed.

## V. SUMMARY AND CONCLUSIONS

In this paper, we have used the  $SU(3) \times SU(3)$  NJL model to calculate temperature dependent cross sections and transition rates in a scheme ordered in the inverse number of colors,  $1/N_c$ . To this end, we have included an exact calculation of the pseudoscalar and scalar meson masses, treating these particles as resonances at temperatures beyond their respective Mott temperatures, when they may dissociate into their constituent quark and antiquark. Our calculation has been performed for finite values of the current quark masses, which is regarded as the physical situation.

In describing the hadronization procedure, we have identified four classes  $u\bar{d}$ ,  $u\bar{s}$ ,  $u\bar{u}$  and  $s\bar{s}$ , determined by the initial incoming quark and antiquark and final states  $\pi\pi$ ,  $\pi K$ ,  $K\bar{K}$ ,  $K\eta$  and  $\eta\eta$ . The individual processes contributing to each class have been listed and calculated, and their contributions to the cross sections have been studied as a function of temperature and centre of mass energy. We are able to account for all the observed structures, that result as a function of (i) threshold effects, (ii) an intermediate resonance being excited, or via the (iii) summation of several processes. The relevance of each process is discussed, and we observe, for example, a forward–backward asymmetry in the class  $u\bar{d} \rightarrow$  hadrons, that is due to the process  $u\bar{d} \rightarrow K^+\bar{K}^0$ . Averaged and total production rates are calculated for each class.

What can be learned from this calculation? From the measured spectra of the hadrons produced in high energy heavy ion collisions, one derives temperatures in the range of 150–200 MeV [16]. This temperature range is also found for the location of the phase transition in lattice gauge calculations. In our calculation, the pion Mott temperature  $T_{M\pi} = 212$  MeV plays the role of separating the regions where pions are stable ( $T < T_{M\pi}$ ) and where they exist as resonances. The unphysical

aspect of our model is the appearance of constituent quarks for  $T < T_{M\pi}$ . Thus all hadronization cross sections for  $T \ll T_{M\pi}$  are only of academic interest. If we focus on the temperature region between 150 MeV and 250 MeV, two (in our opinion) physically relevant numbers can be extracted.

(i) *The hadronization time:* The quark–gluon plasma (if it is reached at all) is a transient state because of the rapid expansion of the system. Therefore it is of great interest to know the times for the various stages of the system: thermalization of the quark–gluon plasma, hadronization and final state interaction time. In our calculation we find an average time for the hadronization of a quark of

$$\tau_{\text{had}} = 2\text{--}4 \text{ fm}/c \quad . \quad (87)$$

This value may be considered not unrealistic in view of expansion scenarios.

(ii) *Strangeness enhancement:* In experiments, a sizeable value of strangeness enhancement  $\Delta K/\pi$  has been observed in heavy ion collisions over  $N + N$  ones. This value is  $\Delta K/\pi = 9\%$ . Our calculation yields an enhancement of about 1% as coming from the hadronization stage. This result indicates that the dominant contribution to strangeness enhancement must occur *before* or *after* hadronization.

On the theoretical side, the present paper shows that hadronization cross sections (as other quantities too) are nonperturbative in nature and have a rather strong temperature dependence. Thus realistic calculations (cascade or other ones) have to take these aspects into consideration, if they want to be realistic.

## ACKNOWLEDGMENTS

We wish to thank P. Zhuang for illuminating discussions. This work has been supported in part by the Deutsche Forschungsgemeinschaft under contract no. Hu 233/4–3, by the Federal Ministry for Education and Research, under contract no. 06 HD 742 and by the EU within the program INTAS (94–2915).

## APPENDIX A: LOOP INTEGRALS

The decomposition of Feynman diagrams into elementary integrals is a well known technique for zero temperature [21]. At finite temperature, however, no

general theory has to date been given. Large  $SU(3)$  calculations are difficult without implementing a technique, that enables one to decompose all expressions into a few integrals only, the calculation of each of which can be done once. The evaluation of these integrals for the general case is a tedious task, which will form the subject of a separate publication [22]. To be concise, we simply illustrate the calculation of the elementary integrals for some special cases here, confining ourselves to the situation of zero chemical potentials and equal masses for all fermions. This is already a sufficient basis for most of the calculations within the two flavor sector. A full calculation, including differing chemical potentials, quark masses, and arbitrary kinematics (applicable in  $C_0$ ) can be found in a forthcoming publication [22]. Since the NJL model is nonrenormalizable, we choose a three momentum cutoff  $\Lambda$  as defining our regularization scheme.

### 1. Computation of $A$

The first loop integral has been defined in Eq. (6) as

$$A(m, \mu) = \frac{16\pi^2}{\beta} \sum_n e^{i\omega_n \eta} \int_{|\vec{p}| < \Lambda} \frac{d^3 p}{(2\pi)^3} \frac{1}{(i\omega_n + \mu)^2 - E^2} , \quad (\text{A1})$$

where  $E = \sqrt{p^2 + m^2}$  and the limit  $\eta \rightarrow 0$  has to be taken after the Matsubara summation. In the case  $\mu = 0$  this is easily evaluated to be

$$A(m, 0) = -4 \int_0^\Lambda dp \frac{p^2}{E} \tanh\left(\frac{\beta E}{2}\right) . \quad (\text{A2})$$

In the limit  $\beta \rightarrow \infty$ , this can be evaluated analytically. For finite temperatures, the integral has to be performed numerically.

### 2. Computation of $B_0$

The second loop integral  $B_0$  is defined as the analytic continuation of

$$B_0(\vec{k}, m_1, \mu_1, m_2, \mu_2, i\nu_m) = \frac{16\pi^2}{\beta} \sum_n e^{i\omega_n \eta} \int_{|\vec{p}| < \Lambda} \frac{d^3 p}{(2\pi)^3} \frac{1}{((i\omega_n + \mu_1)^2 - E_1^2)} \frac{1}{((i\omega_n - i\nu_m + \mu_2)^2 - E_2^2)} \quad (\text{A3})$$

$(E_1 = \sqrt{\vec{p}^2 + m_1^2}, E_2 = \sqrt{(\vec{p} - \vec{k})^2 + m_2^2})$  to the real axis. The case  $\vec{k} = \vec{0}$ , which we require for the determination of the meson masses, is singular and has to be treated separately. For this case, one obtains

$$B_0(\vec{0}, m, 0, m, 0, k_0) = 8\mathcal{P}\int dp \frac{p^2 \tanh\left(\frac{\beta E}{2}\right)}{4E^2 - k_0^2} + i\pi\Theta(k_0 - 2m) \tanh\left(\frac{\beta k_0}{4}\right) \sqrt{1 - \left(\frac{2m}{k_0}\right)^2} . \quad (\text{A4})$$

Here  $\mathcal{P}$  denotes the Cauchy principal value of the integral.

For finite values of  $|\vec{k}|$ ,  $B_0$  takes the form

$$B_0(\vec{k}, m, 0, m, 0, k_0) = -\frac{1}{k} \int_0^\Lambda dp \frac{p \tanh\left(\frac{\beta E}{2}\right)}{E} \left( \log \left| \frac{(k^2 + 2p|\vec{k}|)^2 - 4k_0^2 E^2}{(k^2 - 2p|\vec{k}|)^2 - 4k_0^2 E^2} \right| + i\pi \left( \Theta(2p|\vec{k}| - |k^2 + 2k_0 E|) - \Theta(2p|\vec{k}| - |k^2 - 2k_0 E|) \right) \right) . \quad (\text{A5})$$

The imaginary part of this integral can be easily evaluated analytically. Note that this is not covariant due to our noncovariant regularization scheme.

### 3. Computation of $C_0$

$C_0$  has been defined to be the analytic continuation of

$$C_0(\vec{p}, \vec{k}, m_1, \mu_1, m_2, \mu_2, i\nu_m, m_3, \mu_3, i\alpha_l) = \frac{16\pi^2}{\beta} \sum_n e^{i\omega_n \eta} \int_{|\vec{p}| < \Lambda} \frac{d^3 q}{(2\pi)^3} \times \frac{1}{((i\omega_n + \mu_1)^2 - E_1^2)} \frac{1}{((i\omega_n - i\alpha_l + \mu_2)^2 - E_2^2)} \frac{1}{((i\omega_n - i\nu_m + \mu_3)^2 - E_3^2)} . \quad (\text{A6})$$

In the example presented here, we not only set  $\mu = 0$  and consider equal masses, but also set  $\vec{k} = 0$ ,  $|\vec{q}| = \frac{1}{2}\sqrt{s - 4m_\pi^2}$ ,  $i\alpha_l = \frac{1}{2}\sqrt{s}$  and  $i\nu_m = \sqrt{s}$ . The result can be directly applied to pion production. One finds

$$C_0(\vec{0}, \vec{q}, m, 0, m, 0, \sqrt{s}, m, 0, \frac{1}{2}\sqrt{s}) = -\frac{1}{\sqrt{s(s - 4m_\pi^2)}} \mathcal{P}\int dp \frac{p \tanh\left(\frac{\beta E}{2}\right)}{E} \times \left[ \frac{1}{E} \left( \log \left| \frac{m_\pi^4 - \zeta_-^2}{m_\pi^4 - \zeta_+^2} \right| - i\pi (\Theta(p|\vec{q}| - |\xi_+|) + \Theta(p|\vec{q}| - |\xi_-|)) \right) + \frac{2}{\sqrt{s} - 2E} \left( \log \left| \frac{m_\pi^2 - \zeta_-}{m_\pi^2 - \zeta_+} \right| - i\pi \Theta(p|\vec{q}| - |\xi_-|) \right) \right] . \quad (\text{A7})$$

$$\begin{aligned}
& + \frac{2}{\sqrt{s} + 2E} \left( \log \left| \frac{m_\pi^2 + \zeta_+}{m_\pi^2 + \zeta_-} \right| + i\pi \Theta(p|\vec{q}| - |\xi_+|) \right) \\
& + i\pi \frac{\tanh\left(\frac{\beta\sqrt{s}}{4}\right)}{\sqrt{s(s-4m_\pi^2)}} \left( \log \left| \frac{2m_\pi^2 - (s - |\vec{q}|\sqrt{s-4m^2})}{2m_\pi^2 - (s + |\vec{q}|\sqrt{s-4m^2})} \right| \right. \\
& \quad \left. - i\pi \Theta(|\vec{q}|\sqrt{s-4m^2} - |2m_\pi^2 - s|) \right)
\end{aligned}$$

$(\zeta_\pm = E\sqrt{s} \pm p\sqrt{s-4m_\pi^2}, \xi_\pm = E\sqrt{s} \pm m_\pi^2)$ . In the limit  $m_\pi \rightarrow 0$ , the  $\Theta$  functions vanish identically and Eq. (A7) can be greatly simplified to yield the result of Ref. [12] for the three meson vertex.

For a full calculation of  $B_0$  for arbitrary values of the quark masses and chemical potentials, as well as  $C_0$  for the same and arbitrary kinematics, the reader is referred to Ref. [22].

## APPENDIX B: SQUARED MATRIX ELEMENTS

In this appendix, we give the technical details required for calculating the squared transition amplitude with unspecified general masses. One is required to average over initial states and sum over final states. From the former, one obtains a factor  $1/4N_c^2$ . The color trace gives a factor  $N_c$ . The flavor trace is accounted for explicitly by the factors  $f_s$ ,  $f_t$  and  $f_u$ . Our final expressions for these functions, after taking the spinor trace, are

$$\frac{1}{4N_c^2} \sum_{s,c} |\mathcal{M}_s|^2 = \frac{f_s^2 |g_1 g_2|^2}{2N_c} |\mathcal{D}\Gamma|^2 (s - (m_1 + m_2)^2) \quad (B1)$$

$$\begin{aligned}
\frac{1}{4N_c^2} \sum_{s,c} |\mathcal{M}_t|^2 = & \frac{f_t^2 |g_1 g_2|^2}{2N_c} \frac{1}{(t - m^{(t)2})^2} \left[ (m_3^2 - m_1^2 - t)(t - m_4^2 + m_2^2) \right. \\
& + (m^{(t)2} - t)(s - m_1^2 - m_2^2) + 2m_1 m^{(t)} (t - m_4^2 + m_2^2) \\
& \left. - 2m_2 m^{(t)} (m_3^2 - m_1^2 - t) - 2m_1 m_2 (t + m^{(t)2}) \right] \quad (B2)
\end{aligned}$$

$$\begin{aligned}
\frac{1}{4N_c^2} \sum_{s,c} |\mathcal{M}_u|^2 = & \frac{f_u^2 |g_1 g_2|^2}{2N_c} \frac{1}{(u - m^{(u)2})^2} \left[ (m_4^2 - m_1^2 - u)(u - m_3^2 + m_2^2) \right. \\
& + (m^{(u)2} - u)(s - m_1^2 - m_2^2) + 2m_1 m^{(u)} (u - m_3^2 + m_2^2) \\
& \left. - 2m_2 m^{(u)} (m_4^2 - m_1^2 - u) - 2m_1 m_2 (u + m^{(u)2}) \right] \quad (B3)
\end{aligned}$$

for the squares of the individual channels. Here we denote the masses of the incoming quarks by  $m_1, m_2$ , the masses of the outgoing mesons by  $m_3, m_4$  and the mass of the virtual fermion in the  $t$  and  $u$  channel by  $m^{(t)}$  and  $m^{(u)}$  respectively.

The results for the mixed terms are

$$\frac{1}{4N_c^2} \sum_{s,c} \mathcal{M}_s \mathcal{M}_t^* = -\frac{f_s f_t |g_1 g_2|^2}{2N_c} \frac{\mathcal{D}\Gamma}{t - m^{(t)2}} \left[ m_1(m_2^2 - m_4^2 + t) - m_2(m_3^2 - m_1^2 - t) + m^{(t)}(s - (m_1 + m_2)^2) \right] \quad (\text{B4})$$

$$\frac{1}{4N_c^2} \sum_{s,c} \mathcal{M}_s \mathcal{M}_u^* = -\frac{f_s f_u |g_1 g_2|^2}{2N_c} \frac{\mathcal{D}\Gamma}{u - m^{(u)2}} \left[ m_2(m_1^2 - m_4^2 + u) - m_1(m_3^2 - m_2^2 - u) + m^{(u)}(s - (m_1 + m_2)^2) \right] \quad (\text{B5})$$

$$\begin{aligned} \frac{1}{4N_c^2} \sum_{s,c} \mathcal{M}_t \mathcal{M}_u^* &= \frac{f_t f_u |g_1 g_2|^2}{4N_c} \frac{1}{(t - m^{(t)2})(u - m^{(u)2})} \\ &\times \left[ (m_2^2 + m_3^2 - u)(m_4^2 - m_1^2 + 2m_1 m^{(u)} - u) \right. \\ &\quad + (s - (m_1 - m_2)^2)(m_3^2 + m_4^2 - s) \\ &\quad + (m_2^2 + m_4^2 - t)(m_3^2 - m_1^2 + 2m_1 m^{(t)} - t) \\ &\quad + 2m_2(m_1 - m^{(u)})(m_1^2 + m_3^2 - t) \\ &\quad + 2m_2(m_1 - m^{(t)})(m_1^2 + m_4^2 - u) \\ &\quad \left. + 2(m_1 - m^{(u)})(m_1 - m^{(t)})(s - (m_1 + m_2)^2) \right] . \end{aligned} \quad (\text{B6})$$

From these formulae, it is straightforward to derive the results of Ref. [12] for the case  $m_1 = m_2 = m^{(t)} = m^{(u)}$  and  $m_3 = m_4 = 0$ .

## REFERENCES

- [1] *Proceedings of Quark Matter 1991*, Nucl. Phys. A **544**, 1c (1992).
- [2] *Proceedings of Quark Matter 1993*, Nucl. Phys. A **566**, 1c (1994).
- [3] *Quark-Gluon Plasma*, Ed. R. C. Hwa (World Scientific, Singapore, 1990).
- [4] H. W. Barz, B. L. Friman, J. Knoll and H. Schulz, Nucl. Phys. A **519**, 831 (1990).
- [5] T. S. Biró, P. Lévai and J. Zimányi, Phys. Lett. B **347**, 6 (1995).
- [6] K. Werner, Phys. Rep. **232**, 87 (1993).
- [7] U. Vogl and W. Weise, Prog. Part. Nucl. Phys. **27**, 195 (1991).
- [8] S. P. Klevansky, Rev. Mod. Phys. **64**, 649 (1992).
- [9] T. Hatsuda and T. Kunihiro, Phys. Rep. **247**, 221 (1994).
- [10] F. Karsch in [3].
- [11] W. Zhang and L. Wilets, Phys. Rev. C **45**, 1900 (1992).
- [12] J. Hüfner, S. P. Klevansky, E. Quack and P. Zhuang, Phys. Lett. B **337**, 30 (1994).
- [13] E. Quack and S. P. Klevansky, Phys. Rev. C **49**, 3283 (1994).
- [14] J. Müller and S. P. Klevansky, Phys. Rev. C **50**, 410 (1994).
- [15] V. Dmitrašinović, H. J. Schulze, R. Tegen and R. H. Lemmer, Ann. Phys. (NY) **238**, 332 (1995).
- [16] T. Alber et al., Z. Phys. C **64**, 195 (1994).
- [17] P. Zhuang, J. Hüfner and S. P. Klevansky, Nucl. Phys. A **576**, 525 (1994).
- [18] S. R. de Groot, W. A. van Leeuwen and Ch. G. van Weert, *Relativistic Kinetic Theory* (North Holland, Amsterdam, 1980).
- [19] P. Koch, B. Müller and J. Rafelski, Phys. Rep. **142**, 167 (1986).

- [20] *Proc. Int. Symposium on Strangeness in Hadronic Matter*, Nucl. Phys. A **479**, 1c (1988).
- [21] G. J. van Oldenborgh and J. A. M. Vermaseren, Z. Phys. C **46**, 425 (1990) and references cited therein.
- [22] P. Rehberg and S. P. Klevansky, in preparation.

## FIGURES

FIG. 1. The  $q\bar{q}$  scattering amplitude in the random phase approximation.

FIG. 2. Feynman diagram for the irreducible pseudoscalar polarization function.

FIG. 3. Temperature dependence of the constituent quark masses. The solid line refers to the light quarks up and down, the dashed line to the strange quark.

FIG. 4. Temperature dependence of the pseudoscalar meson masses, as well as that of  $2m_q$  and  $m_q + m_s$ . Respective Mott temperatures are indicated by the solid points.

FIG. 5. Temperature dependence of the pion (solid line) and kaon (dashed line) coupling strengths.

FIG. 6. Temperature dependence of the scalar meson masses and  $2m_q$ .

FIG. 7. Generic form of Feynman graphs for the hadronization amplitudes to leading order in  $1/N_c$ . Quarks are denoted by single lines, mesons by double ones. The three diagrams represent  $s$  channel,  $t$  channel and  $u$  channel exchanges, respectively.

FIG. 8. Three meson vertex,  $\Gamma(i\nu_m, \vec{k}; i\alpha_l, \vec{p})$ .

FIG. 9. Feynman graphs for the process  $u\bar{d} \rightarrow \pi^+ \pi^0$ .

FIG. 10. Feynman graphs for the process  $u\bar{s} \rightarrow \pi^+ K^0$ .

FIG. 11. Feynman graphs for the process  $u\bar{u} \rightarrow \pi^+ \pi^-$ .

FIG. 12. Decomposition of the rate for  $u\bar{d} \rightarrow \pi^+ \eta$  at  $T = 0$  into its individual contributions. At the threshold, the  $t$  channel contribution is finite, the vertical line indicating the position of the threshold.

FIG. 13. Contributions of individual hadronization processes for  $u\bar{d} \rightarrow$  hadrons at  $T = 0$ . The contribution of the process  $u\bar{d} \rightarrow \pi^+\eta'$  is negligible and is thus not shown. The rate for  $u\bar{d} \rightarrow \pi^+\pi^0$  is finite at threshold, which is indicated by the vertical line.

FIG. 14. Transition rates for  $u\bar{d} \rightarrow$  hadrons at various temperatures. Solid line:  $T = 0$ , dashed line:  $T = 150$  MeV, dotted line:  $T = 190$  MeV, dot-dashed line:  $T = 250$  MeV. At  $T = 0$  and  $T = 150$  MeV, the vertical line indicates a finite rate at threshold.

FIG. 15. Differential hadronization cross section for  $u\bar{d} \rightarrow$  hadrons at  $T = 0$ ,  $\sqrt{s} = 1.5$  GeV.

FIG. 16. Contributions of individual hadronization processes for  $u\bar{s} \rightarrow$  hadrons at  $T = 0$ . The contribution of the process  $u\bar{s} \rightarrow K^+\eta'$  is negligible and is thus not shown. The contributions of the processes  $u\bar{s} \rightarrow \pi^+K^0$  and  $u\bar{s} \rightarrow \pi^0K^+$  are finite at threshold.

FIG. 17. Transition rates for  $u\bar{s} \rightarrow$  hadrons at various temperatures. Solid line:  $T = 0$ , dashed line:  $T = 150$  MeV, dotted line:  $T = 190$  MeV, dot-dashed line:  $T = 250$  MeV. At  $T = 0$  and  $T = 150$  MeV, the vertical line indicates a finite rate at threshold.

FIG. 18. Contributions of individual hadronization processes for  $u\bar{u} \rightarrow$  hadrons at  $T = 0$ . Only the four dominant processes are shown. The contribution of the process  $u\bar{u} \rightarrow \pi^+\pi^-$  is finite at threshold.

FIG. 19. Transition rates for  $u\bar{u} \rightarrow$  hadrons at various temperatures. Solid line:  $T = 0$ , dashed line:  $T = 150$  MeV, dotted line:  $T = 190$  MeV, dot-dashed line:  $T = 250$  MeV. At  $T = 0$  and  $T = 150$  MeV, the vertical line indicates a finite rate at threshold.

FIG. 20. Contributions of the dominant individual hadronization processes for  $s\bar{s} \rightarrow$  hadrons at  $T = 0$ . The contributions of the processes  $s\bar{s} \rightarrow K^+K^-$  and  $s\bar{s} \rightarrow K^+K^-$  are finite at threshold, as indicated by the vertical line.

FIG. 21. Transition rates for  $s\bar{s} \rightarrow$  hadrons at various temperatures. Solid line:  $T = 0$ , dashed line:  $T = 150$  MeV, dotted line:  $T = 190$  MeV, dot-dashed line:  $T = 250$  MeV. At  $T = 0$  and  $T = 150$  MeV, the vertical line indicates a finite rate at threshold.

FIG. 22. Temperature dependence of the averaged transition rates  $\bar{w}(T)$ . Solid line:  $u\bar{d} \rightarrow$  hadrons, dashed line:  $u\bar{s} \rightarrow$  hadrons, dotted line:  $u\bar{u} \rightarrow$  hadrons, dot-dashed line:  $s\bar{s} \rightarrow$  hadrons.

FIG. 23. Temperature dependence of hadronization times for light quarks (solid line) and strange quarks (dashed line). Note the broken scale on the abscissa.

FIG. 24. Temperature dependence of the averaged strangeness production/destruction rates. Solid line:  $u\bar{d} \rightarrow$  strange hadrons, dashed line:  $u\bar{u} \rightarrow$  strange hadrons, dot-dashed line:  $s\bar{s} \rightarrow$  nonstrange hadrons.

FIG. 25. Temperature dependence of the strangeness enhancement factor  $(\Delta K)_{\text{gain}}/\pi$  (solid line) and the strangeness reduction factor  $(\Delta K)_{\text{loss}}/\pi$  (dashed line).

## TABLES

TABLE I. The four independent incoming  $q\bar{q}$  states and their associated outgoing two meson states.

incoming	$u\bar{d}$	$u\bar{s}$	$u\bar{u}$	$s\bar{s}$
outgoing	$\pi^+\pi^0$ $K^+\overline{K^0}$ $\pi^+\eta$ $\pi^+\eta'$	$\pi^+K^0$ $\pi^0K^+$ $\eta K^+$ $\eta' K^+$	$\pi^+\pi^-$ $\pi^0\pi^0$ $K^+K^-$ $K^0\overline{K^0}$ $\pi^0\eta$ $\pi^0\eta'$ $\eta\eta'$ $\eta\eta$ $\eta'\eta'$	$\pi^+\pi^-$ $\pi^0\pi^0$ $K^+K^-$ $K^0\overline{K^0}$ $\eta\eta'$ $\eta\eta$ $\eta'\eta'$

Figure 3

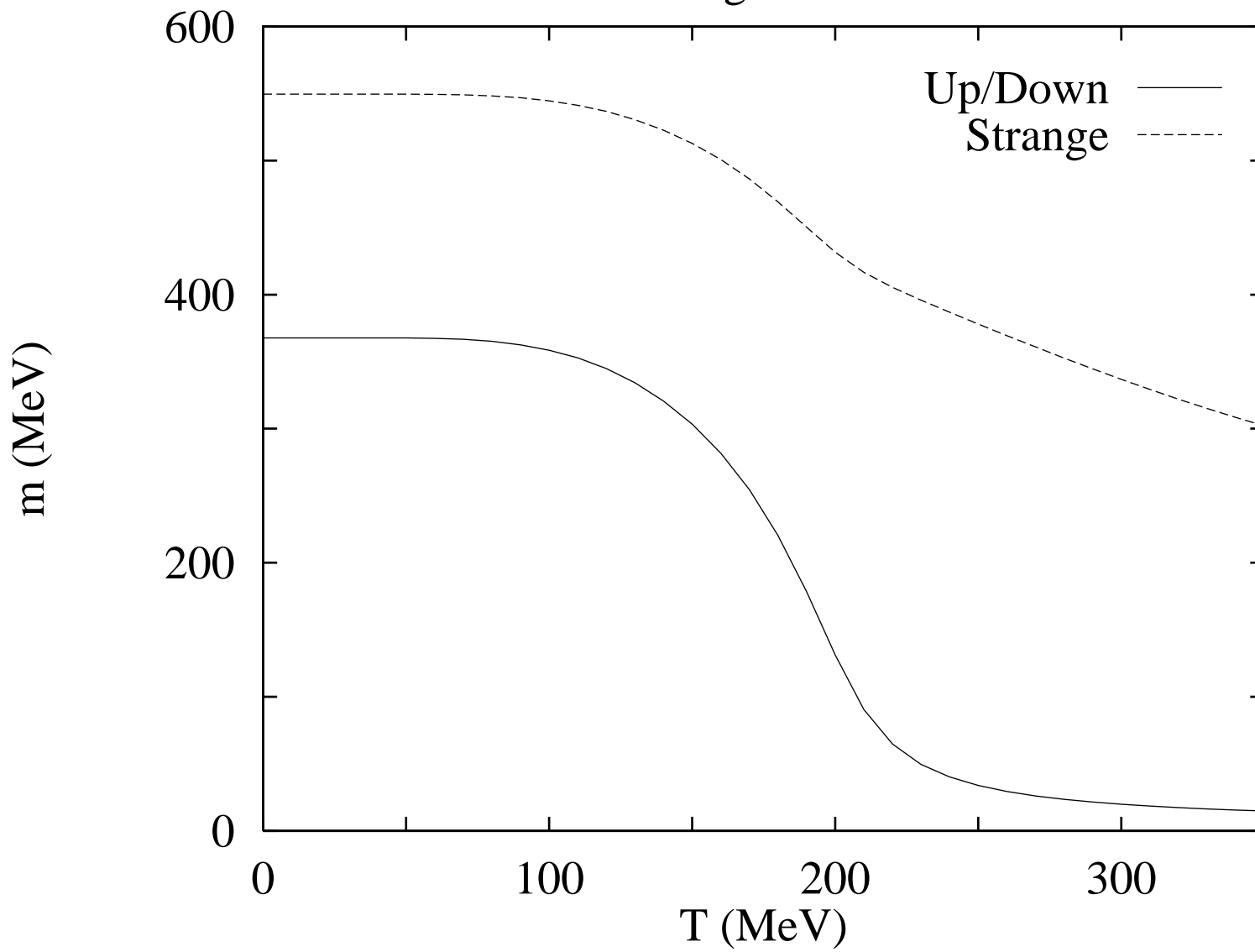


Figure 4

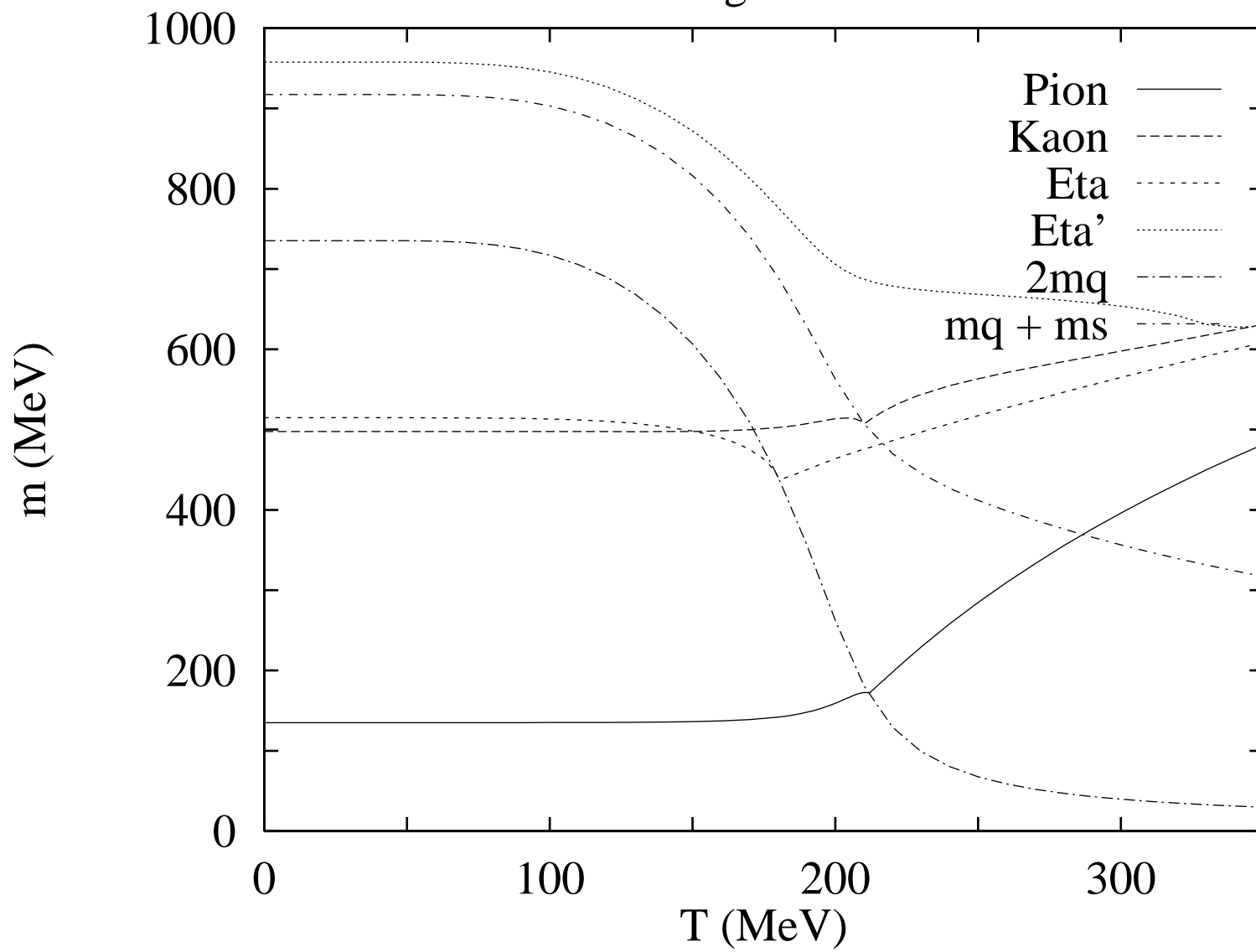


Figure 5

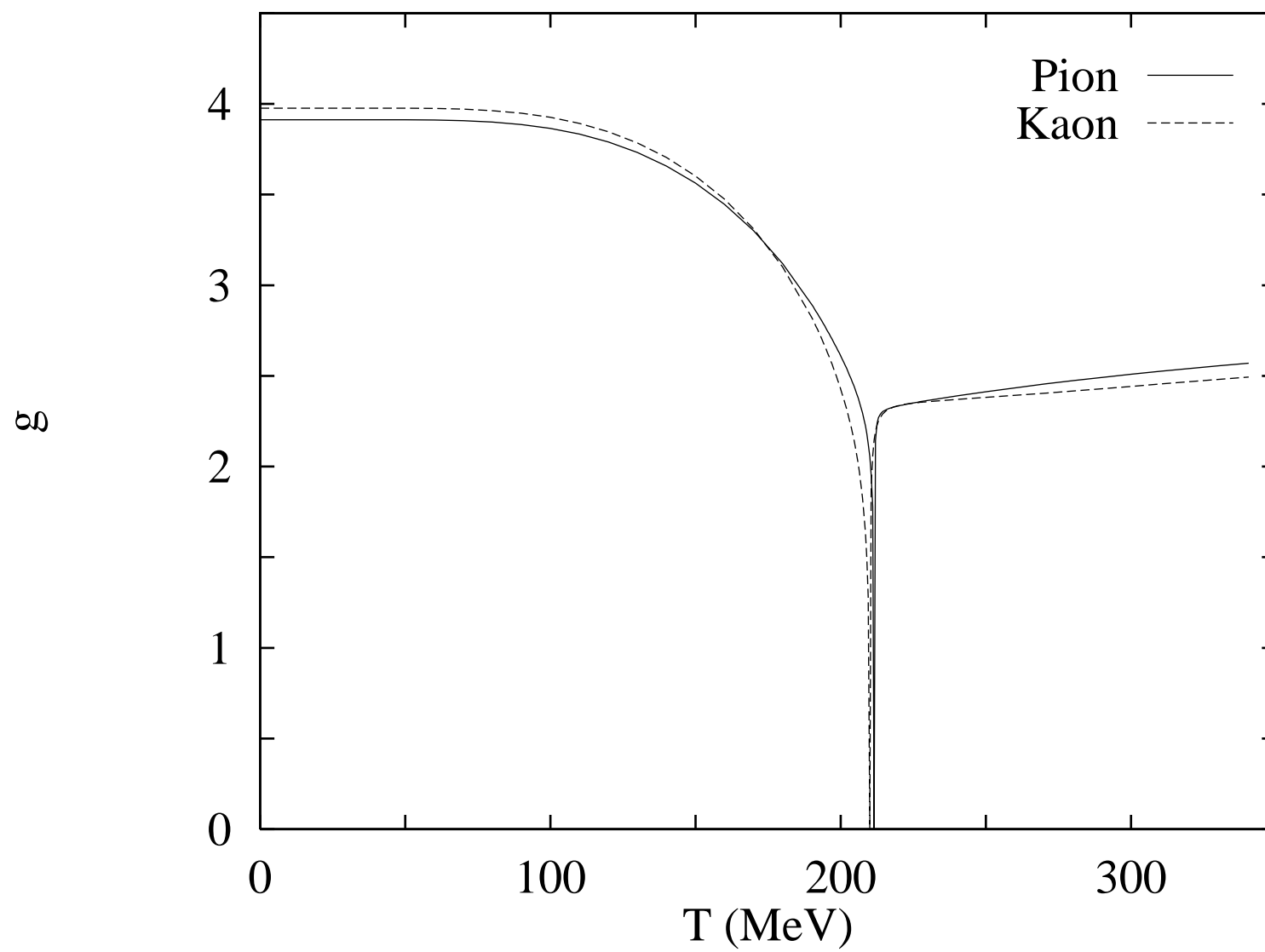


Figure 6

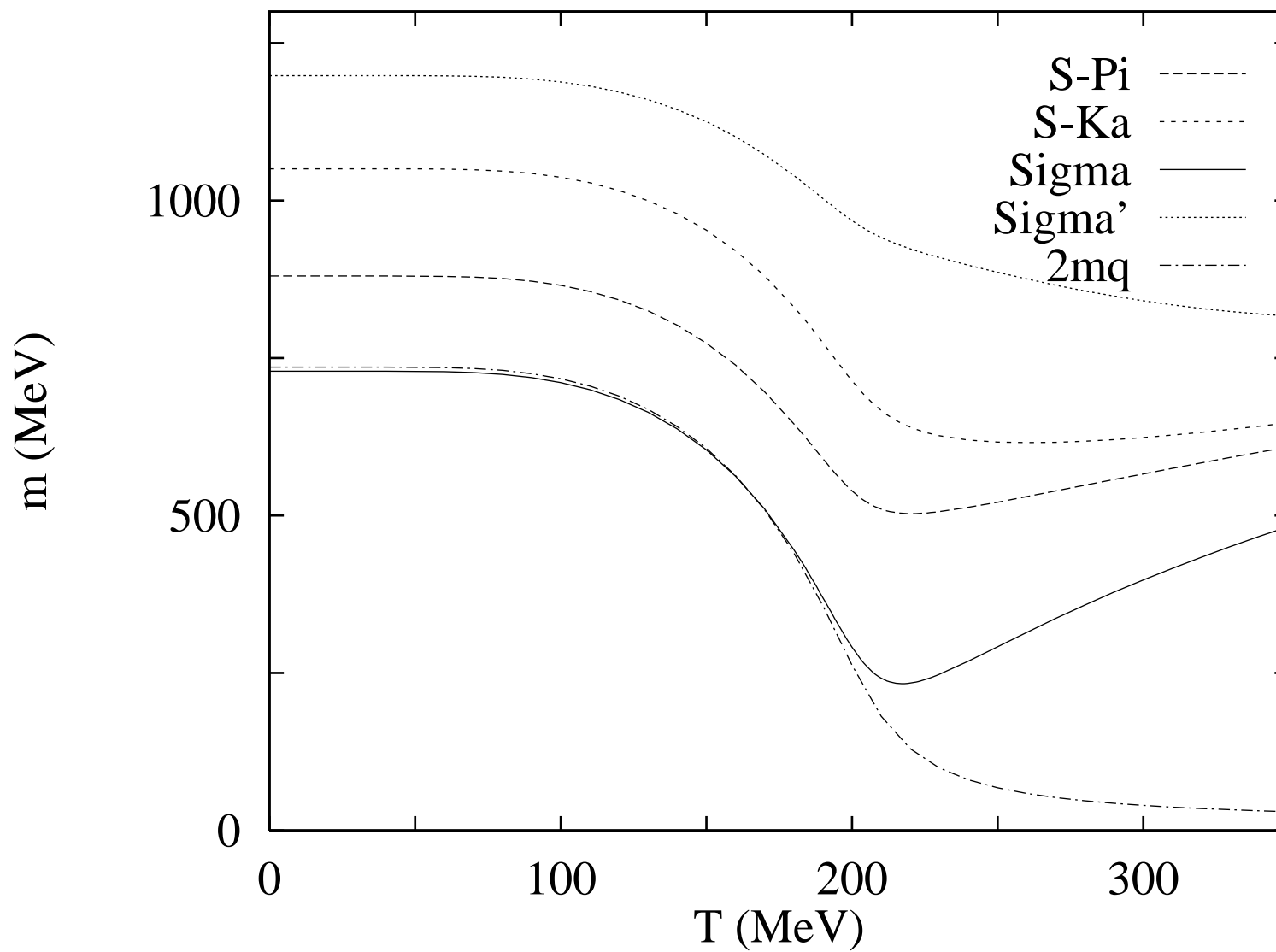


Figure 12

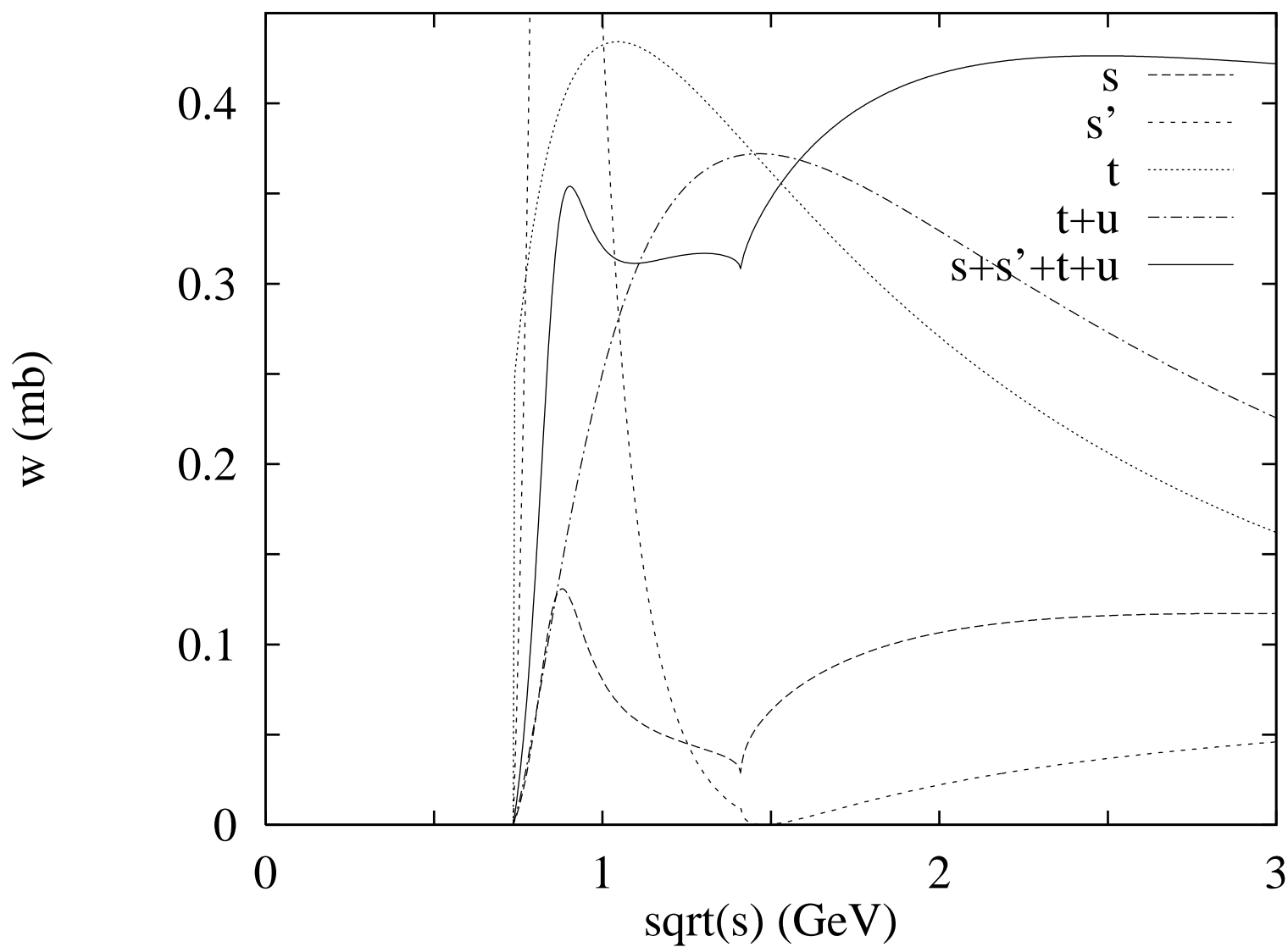


Figure 13

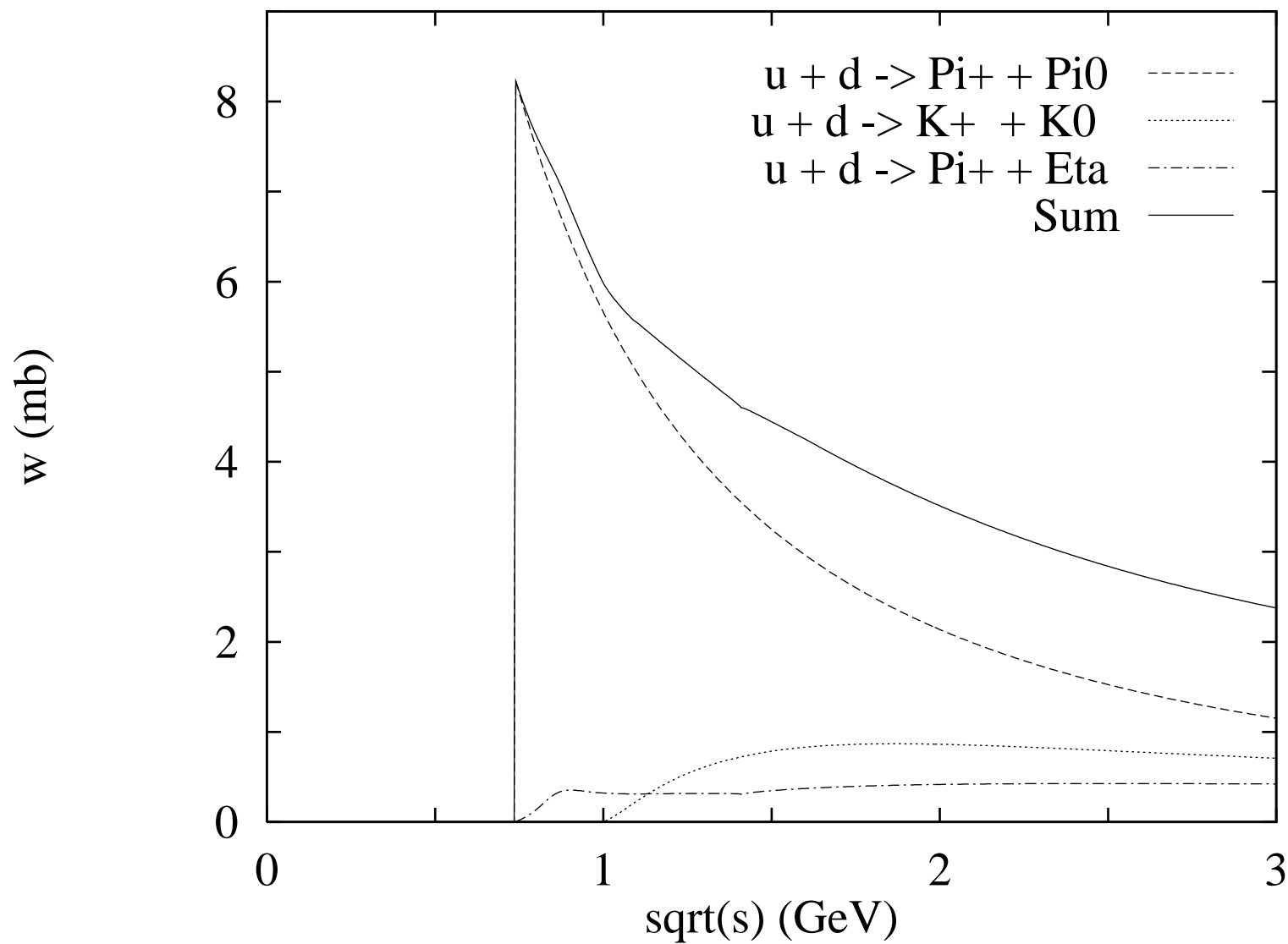


Figure 14

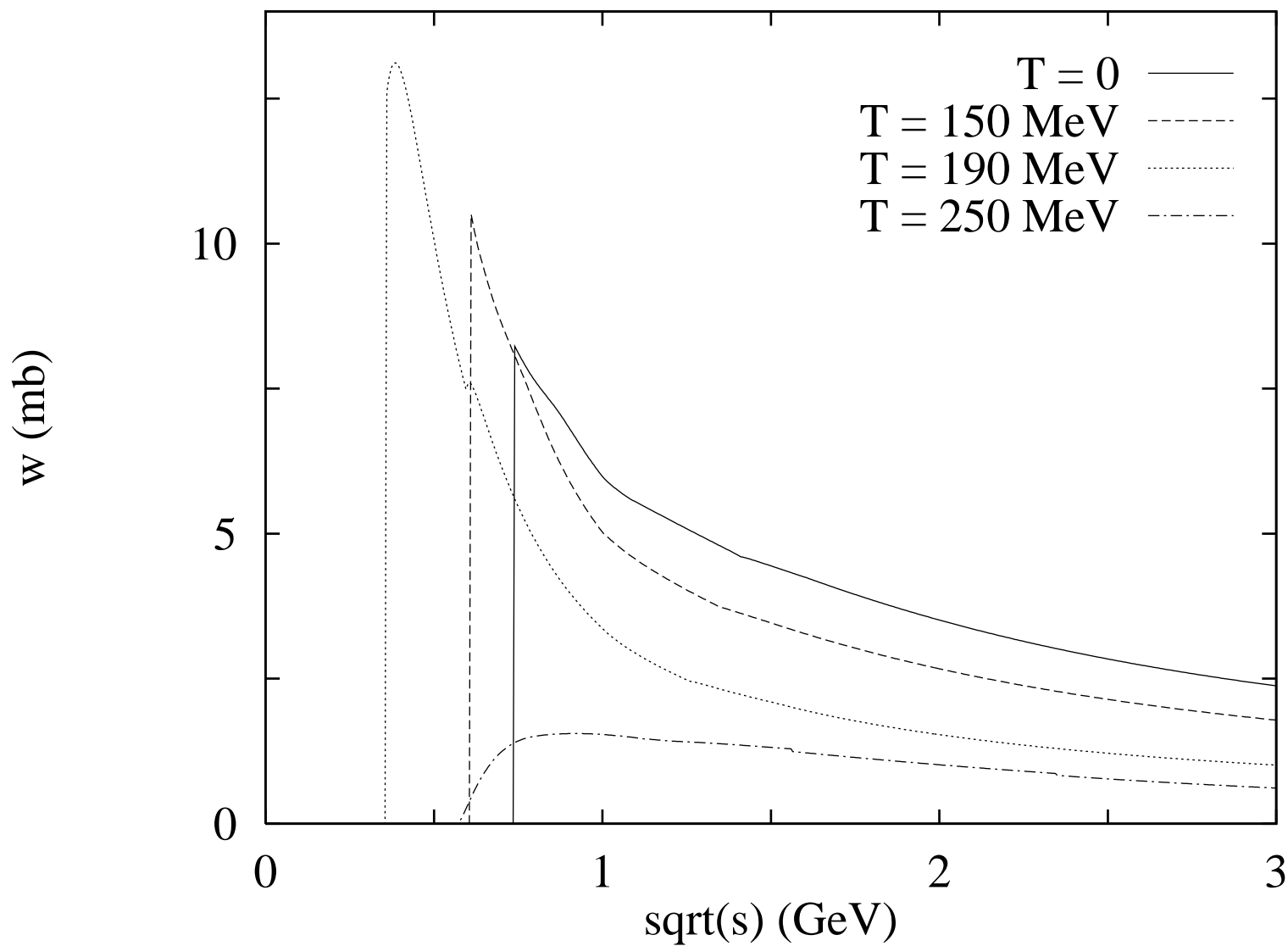


Figure 15

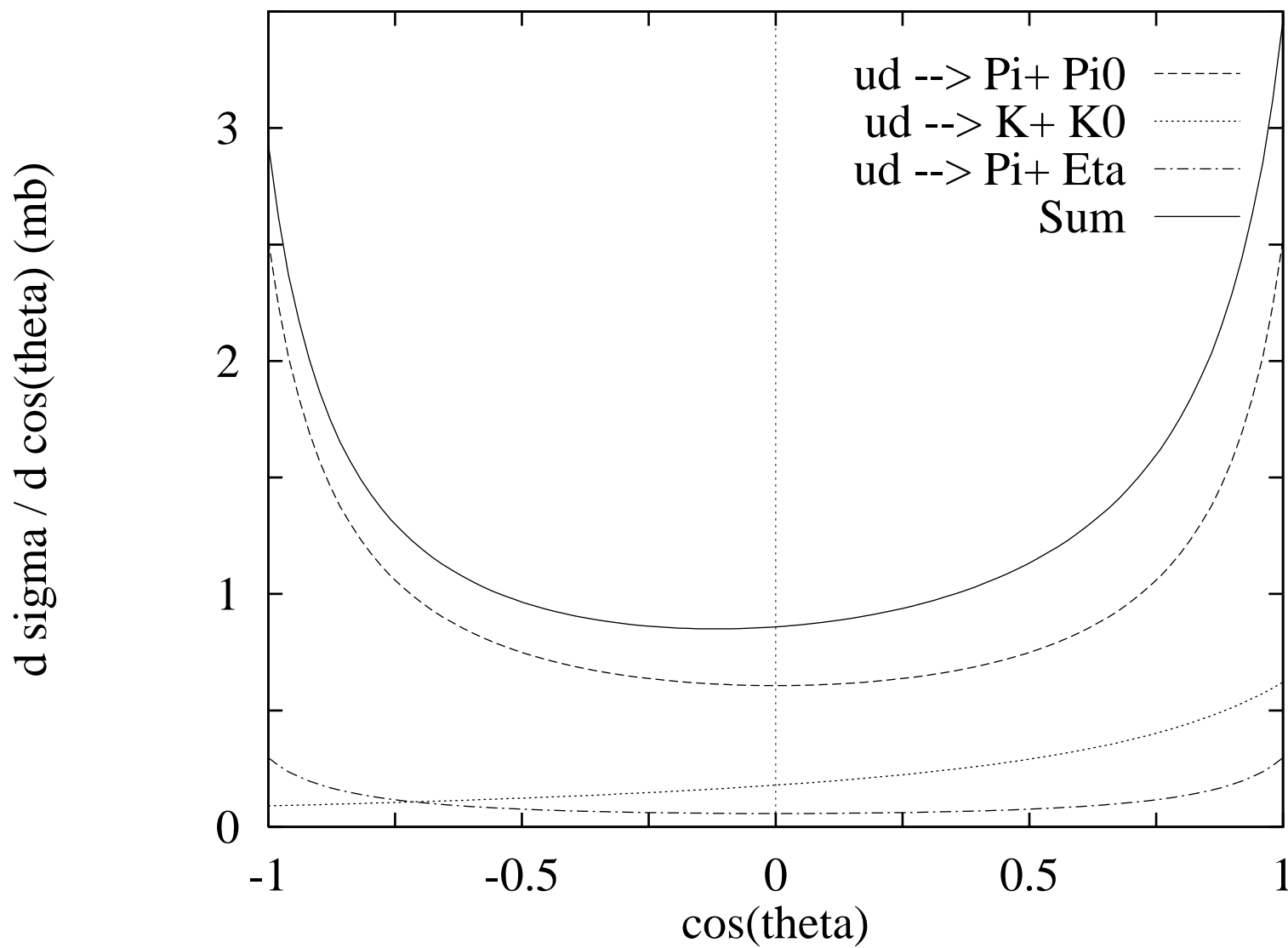


Figure 16

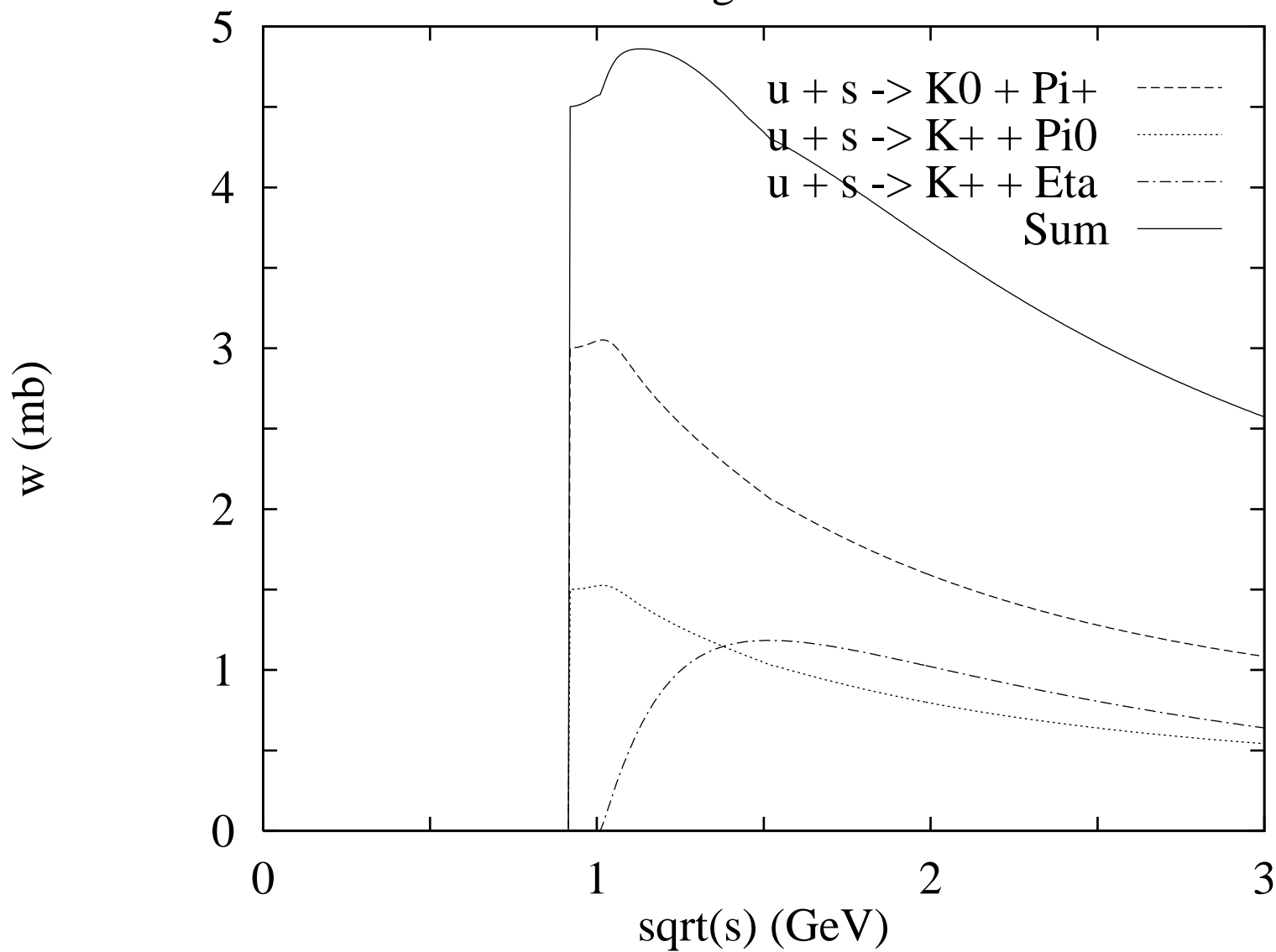


Figure 17

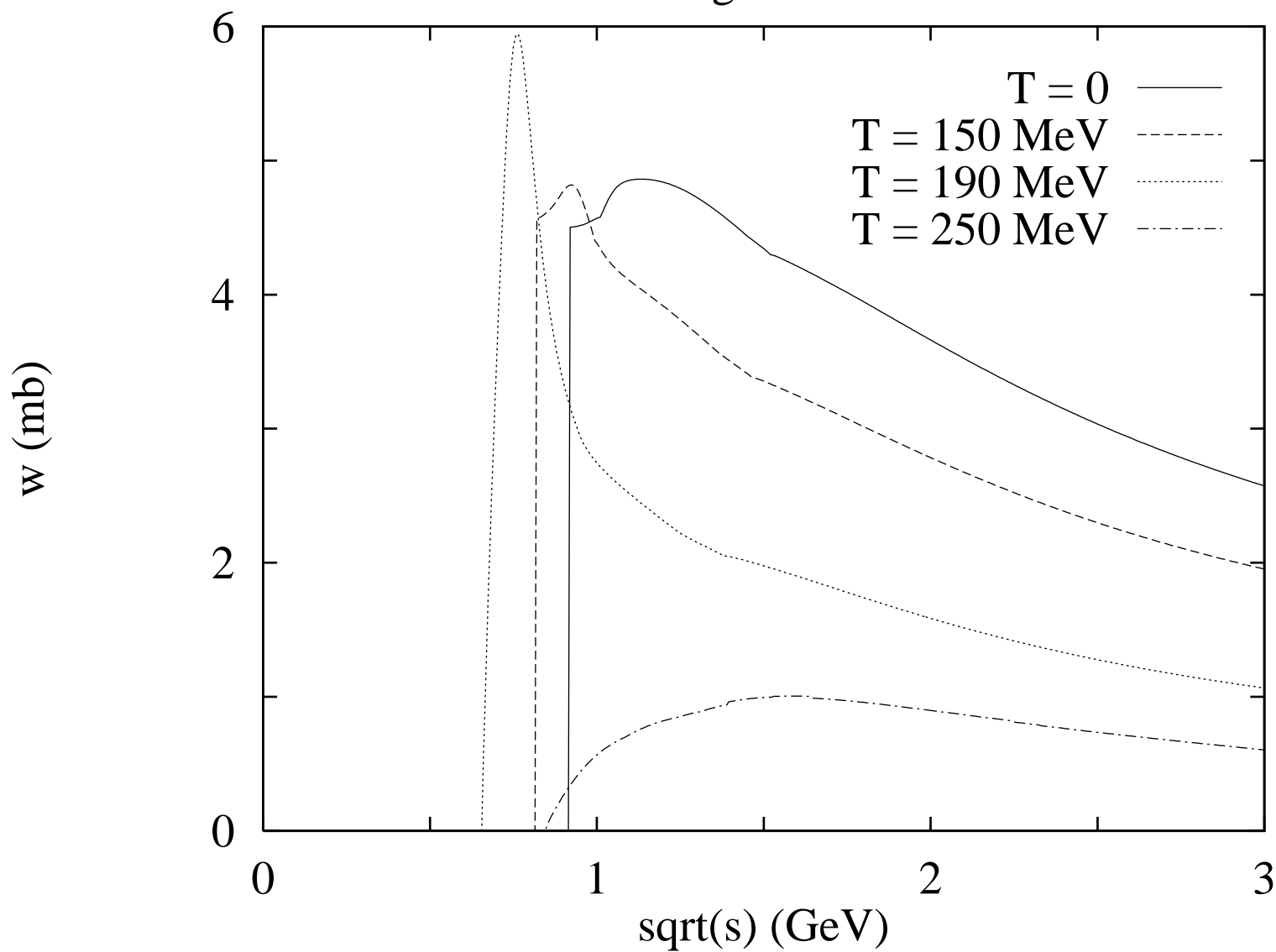


Figure 18

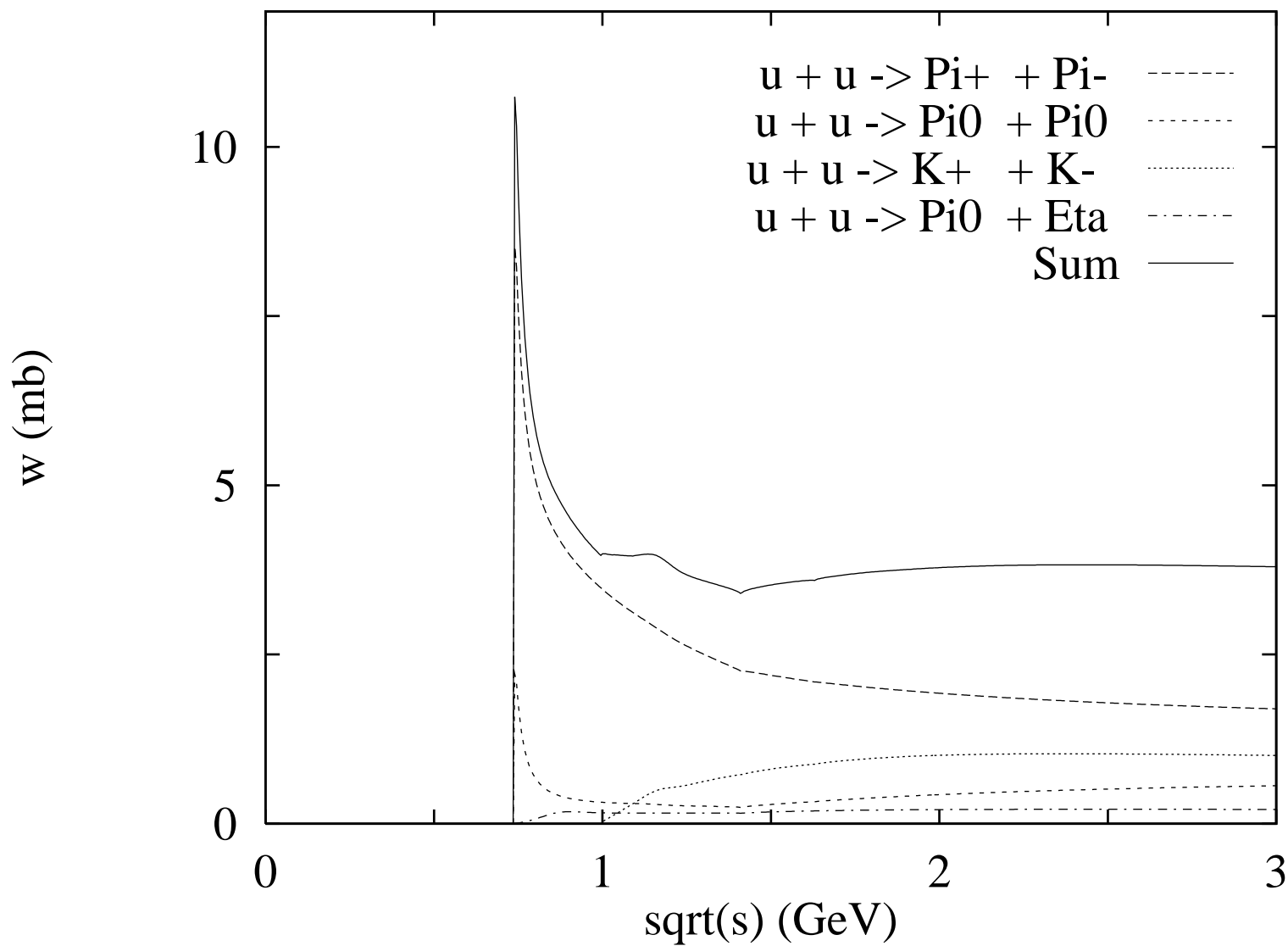


Figure 19

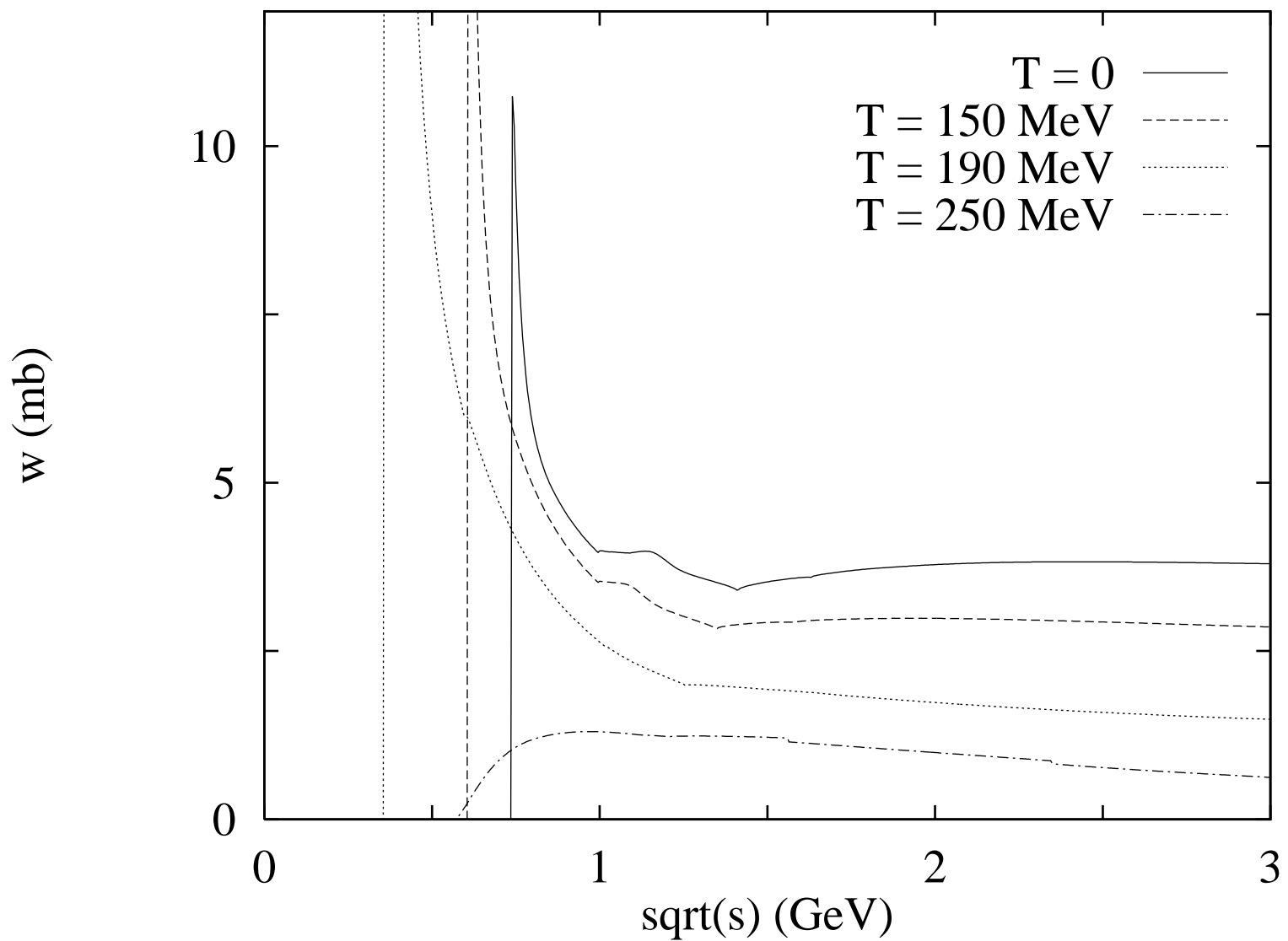


Figure 20

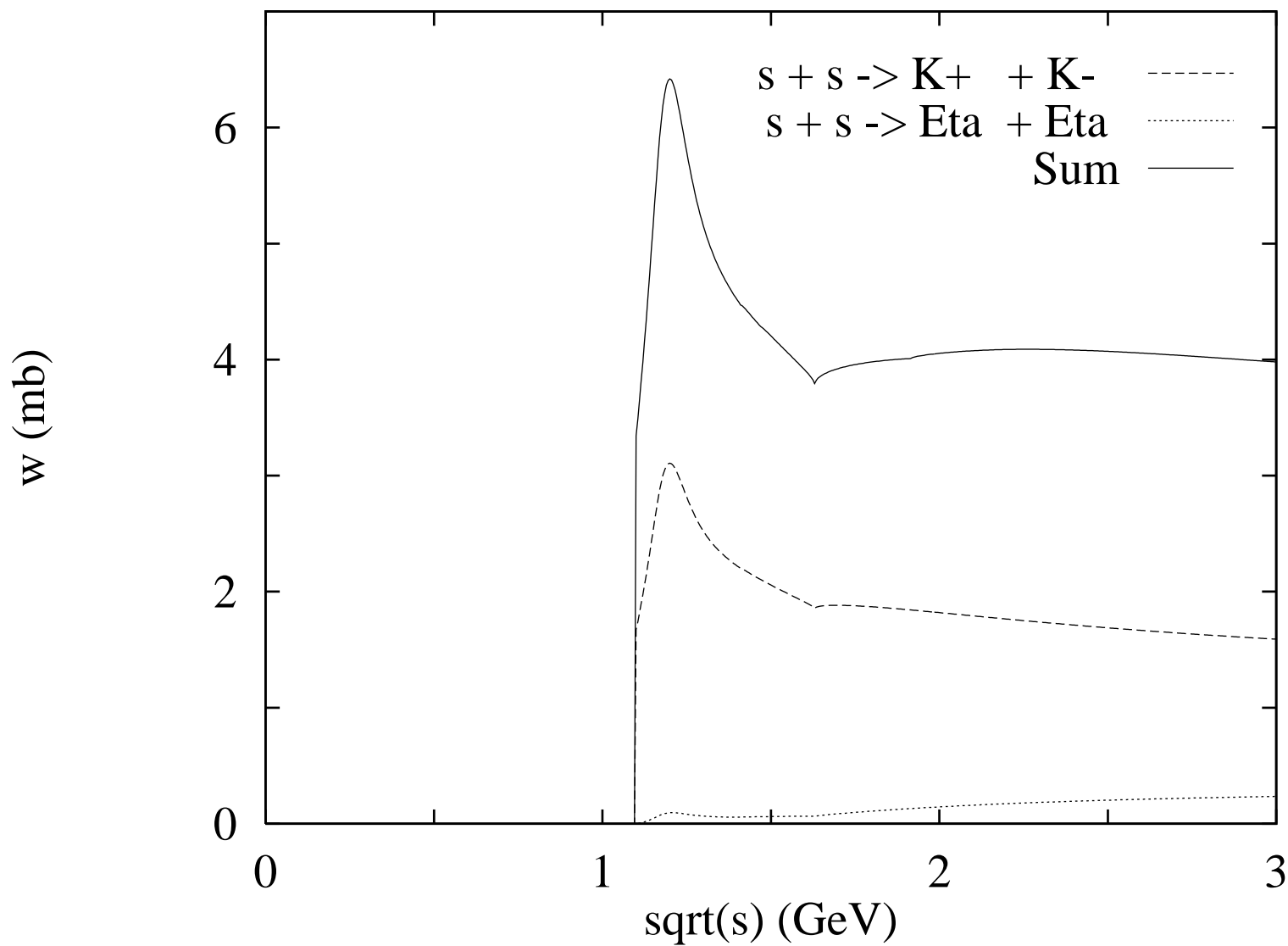


Figure 21

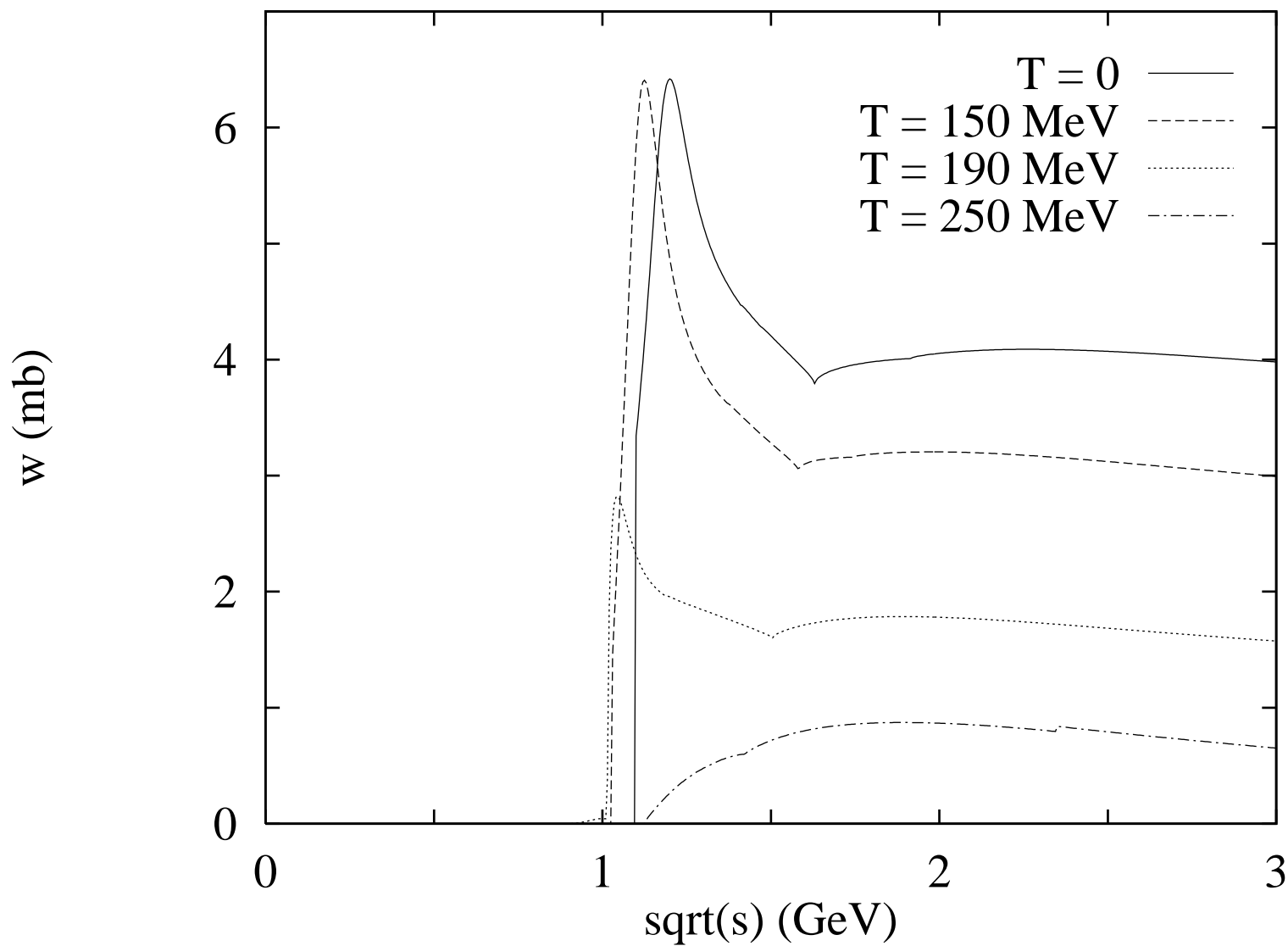


Figure 22

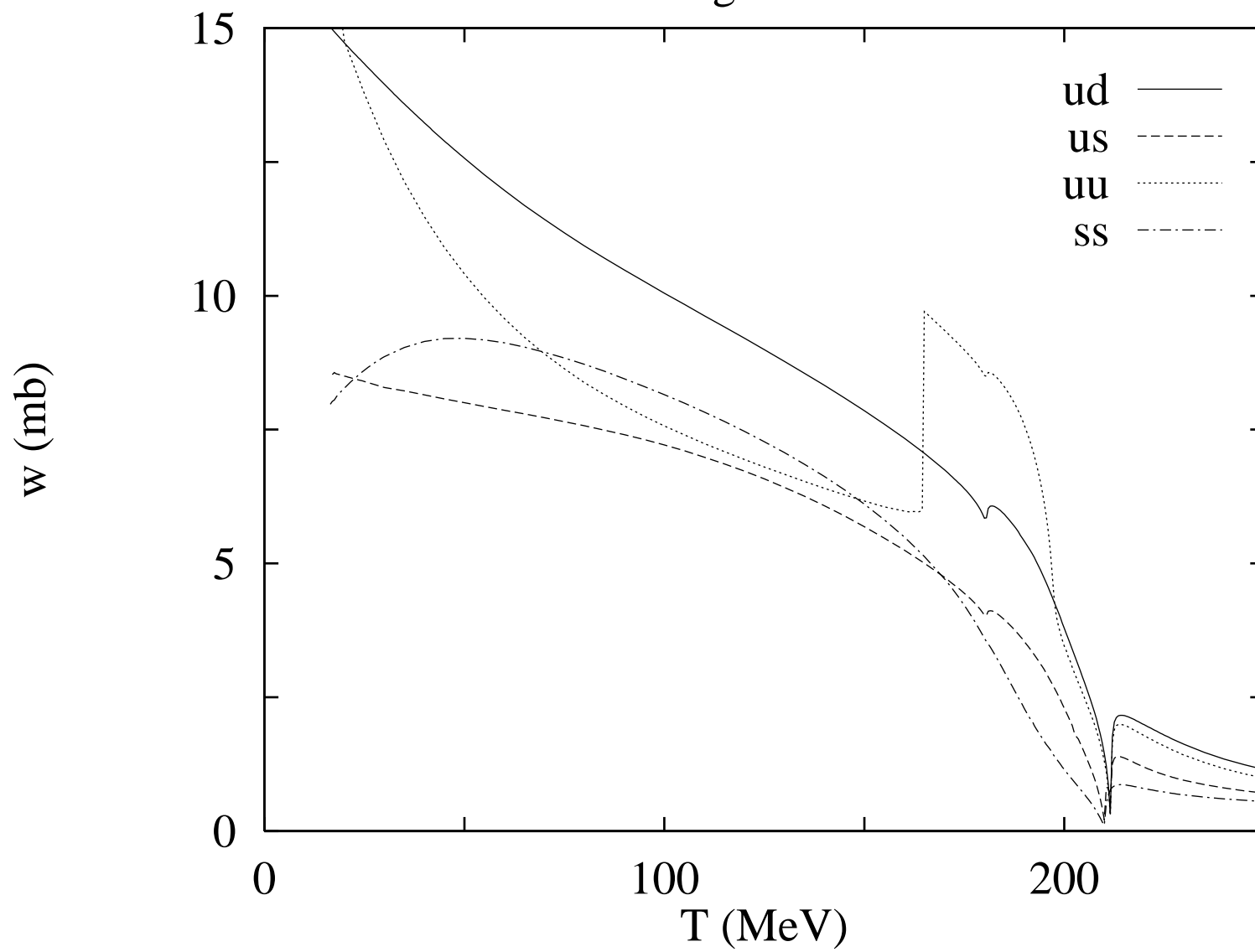


Figure 23

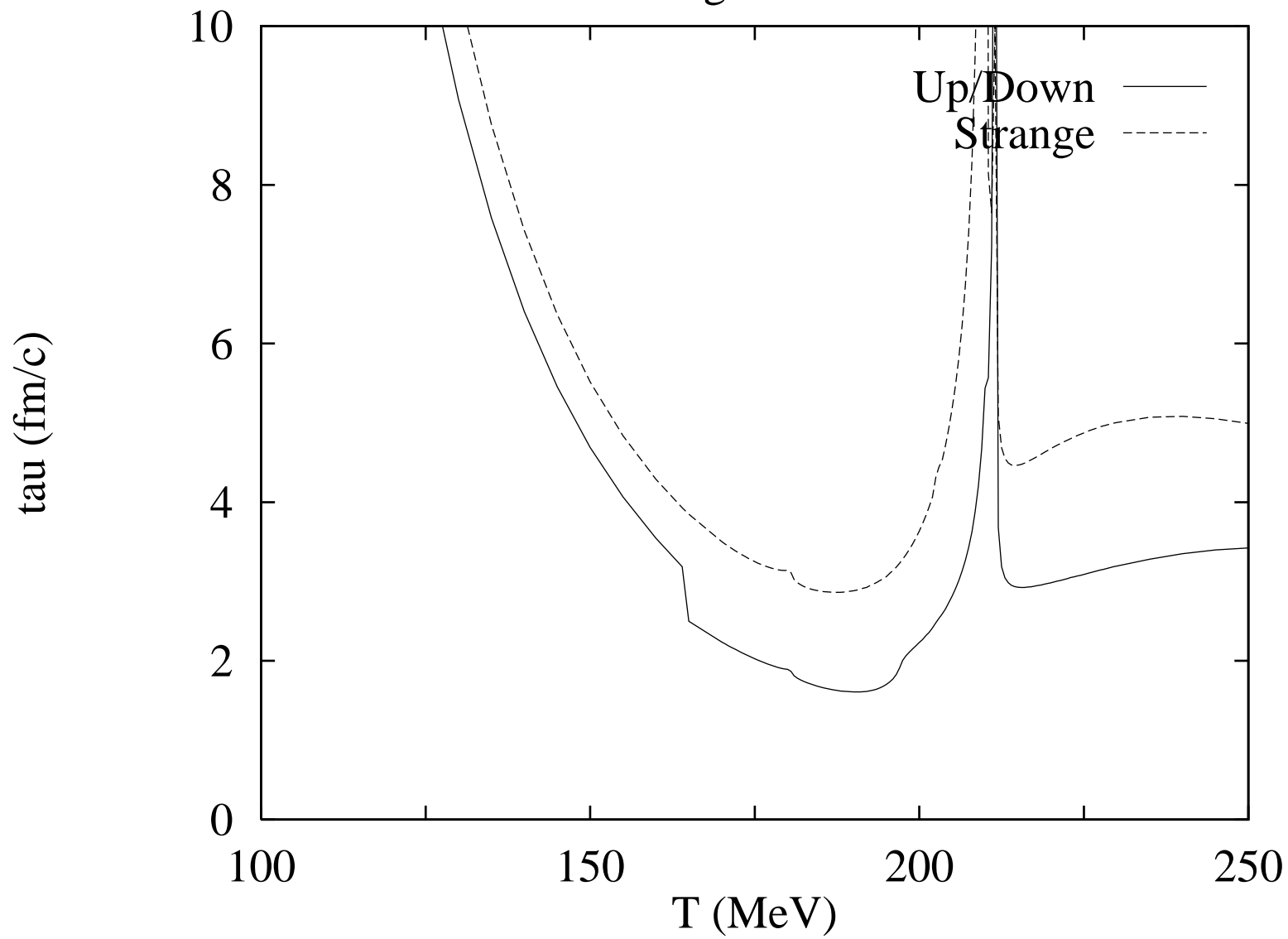


Figure 24

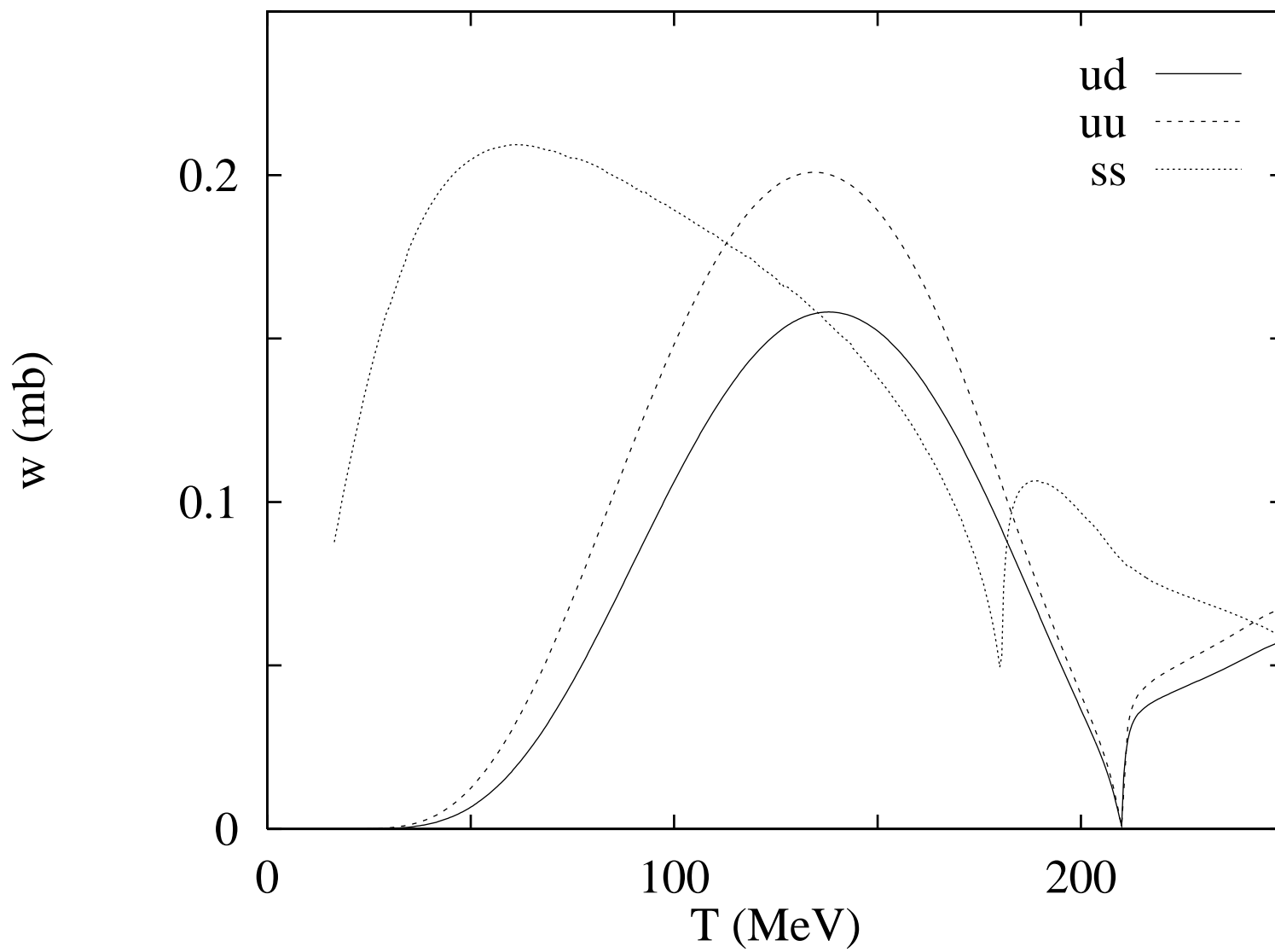
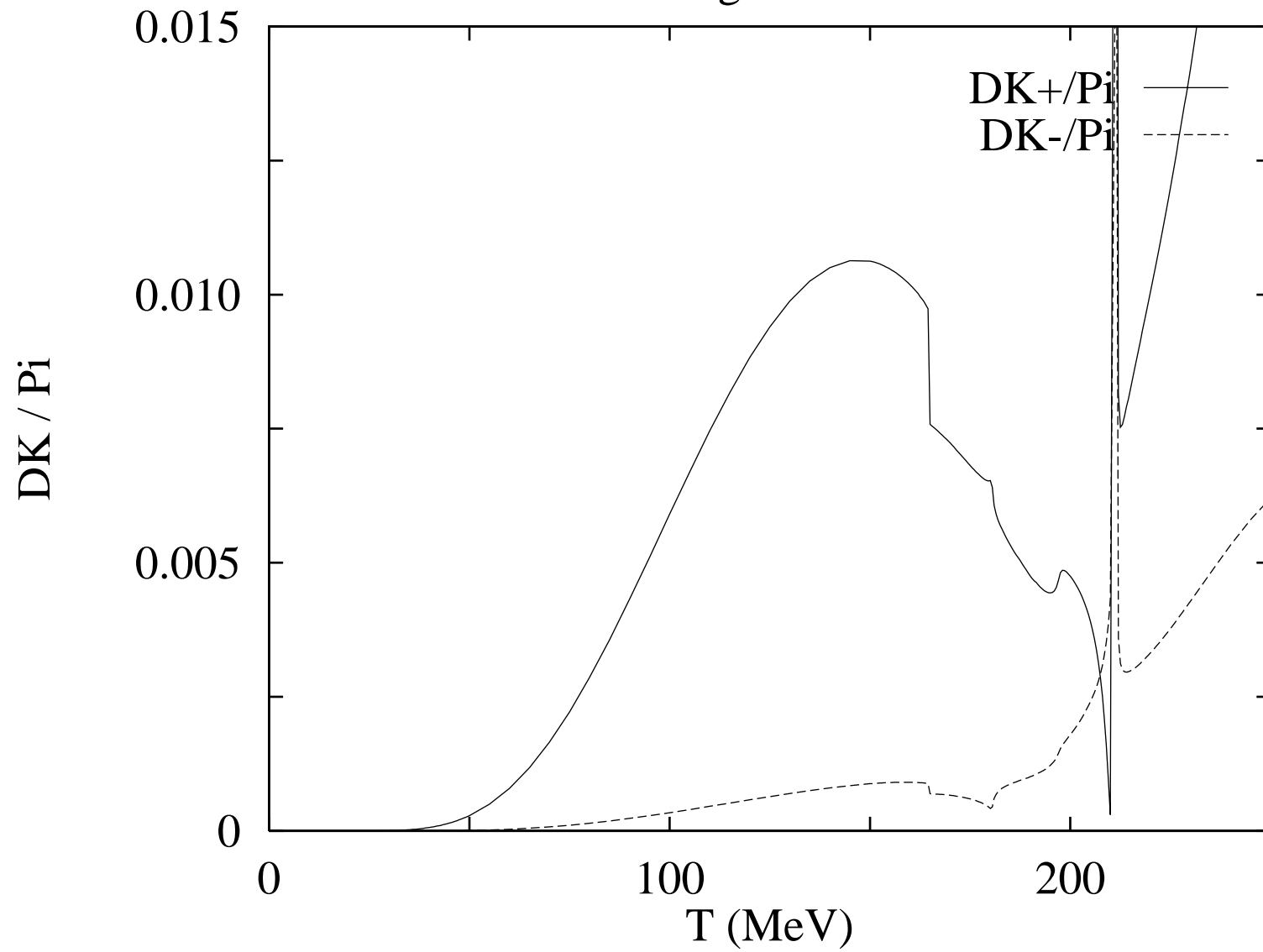


Figure 25



$$iM = \begin{array}{c} \text{Diagram of two intersecting lines} \end{array} + \begin{array}{c} \text{Diagram of two intersecting lines with a central circle} \end{array} + \dots$$

$$\begin{array}{c} \text{Diagram of two intersecting lines with two central circles} \end{array} + \dots$$

Figure 1

$$-i\Pi^P(i\nu_m, \vec{k}) = \begin{array}{c} m_1, \mu_1 \\ (i\omega_n, \vec{p}) \end{array} \begin{array}{c} \rightarrow \\ \text{---} \\ \text{---} \\ \text{---} \\ \text{---} \end{array} \begin{array}{c} i\gamma_5 \\ \text{---} \\ \text{---} \\ \text{---} \\ \text{---} \end{array} \begin{array}{c} \leftarrow \\ \text{---} \\ \text{---} \\ \text{---} \\ \text{---} \end{array} \begin{array}{c} m_2, \mu_2 \\ (i\omega_n - i\nu_m, \vec{p} - \vec{k}) \end{array}$$

Figure 2

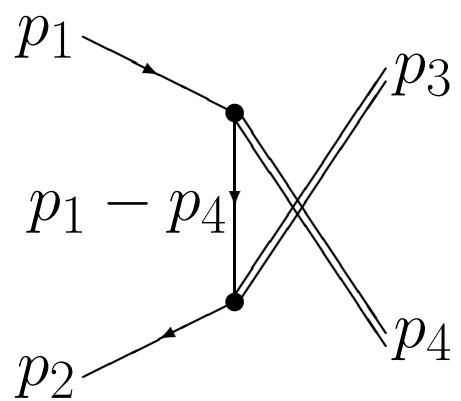
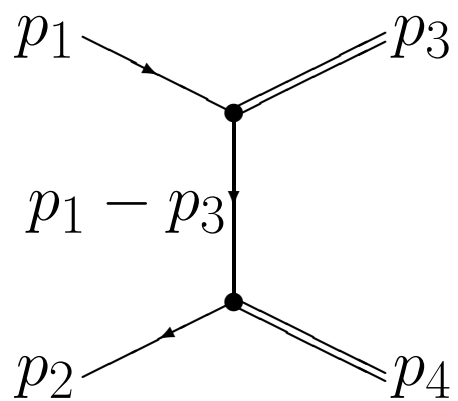
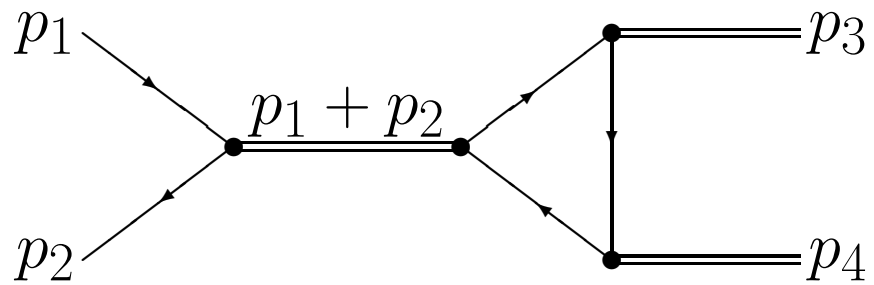


Figure 7

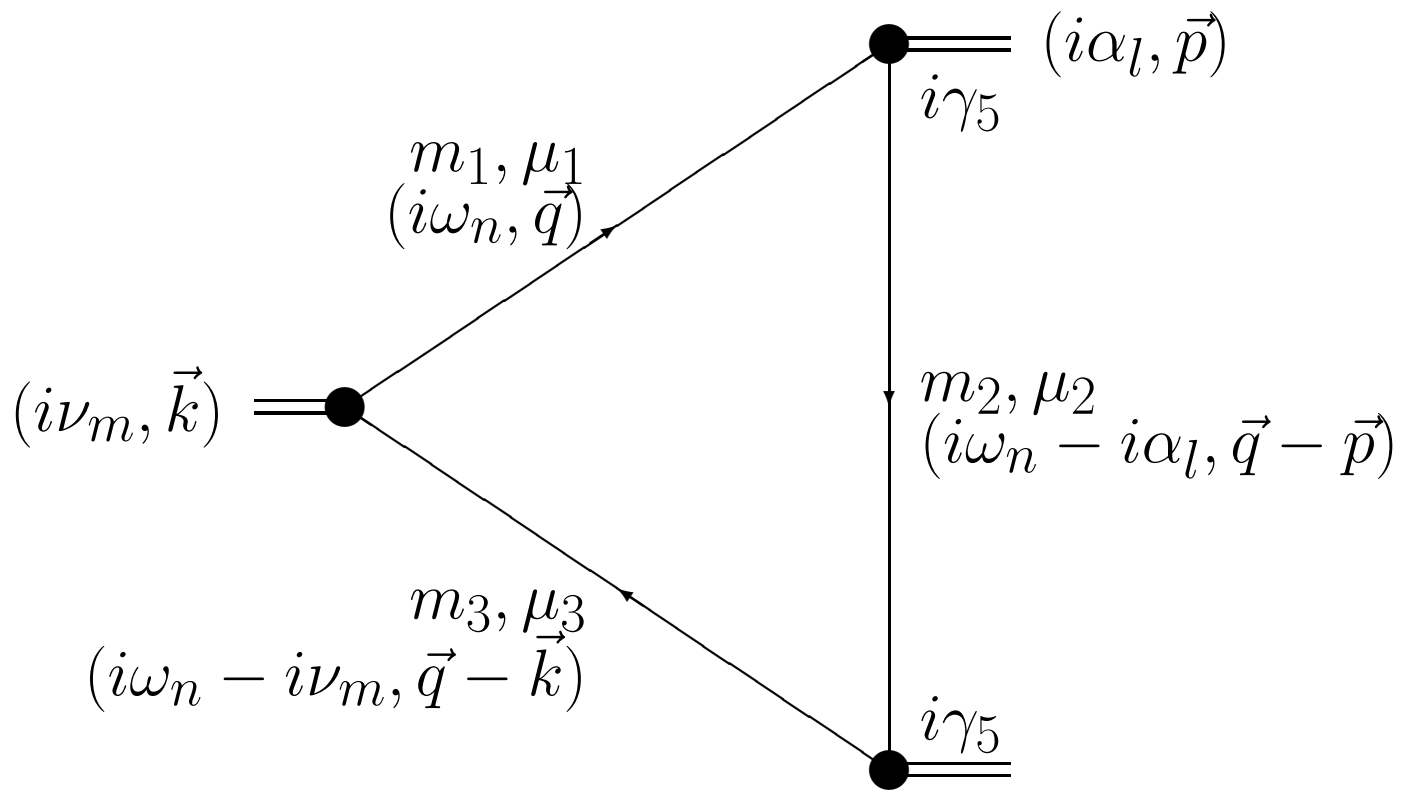


Figure 8

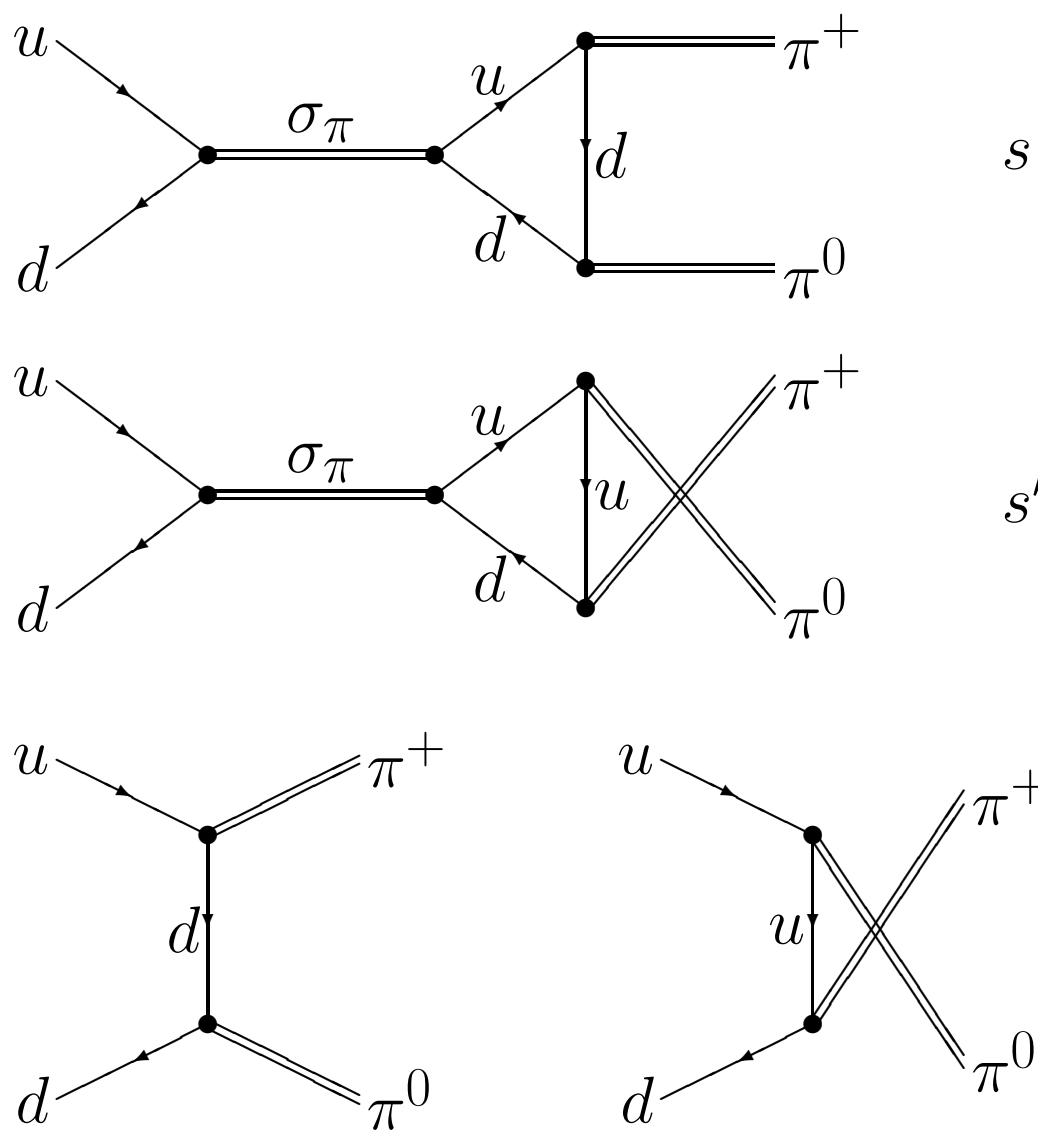


Figure 9

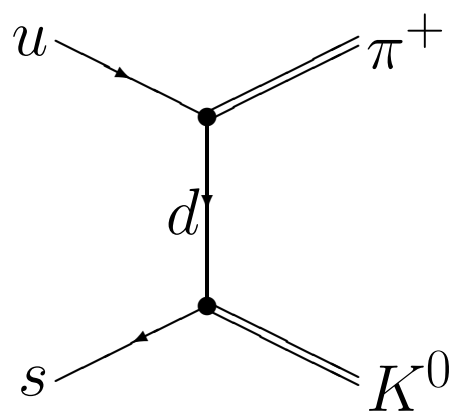
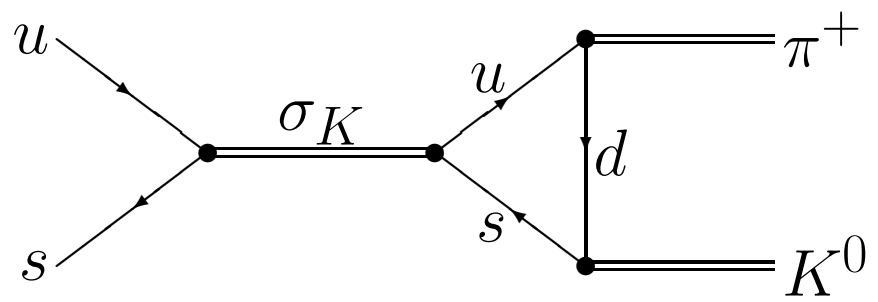


Figure 10

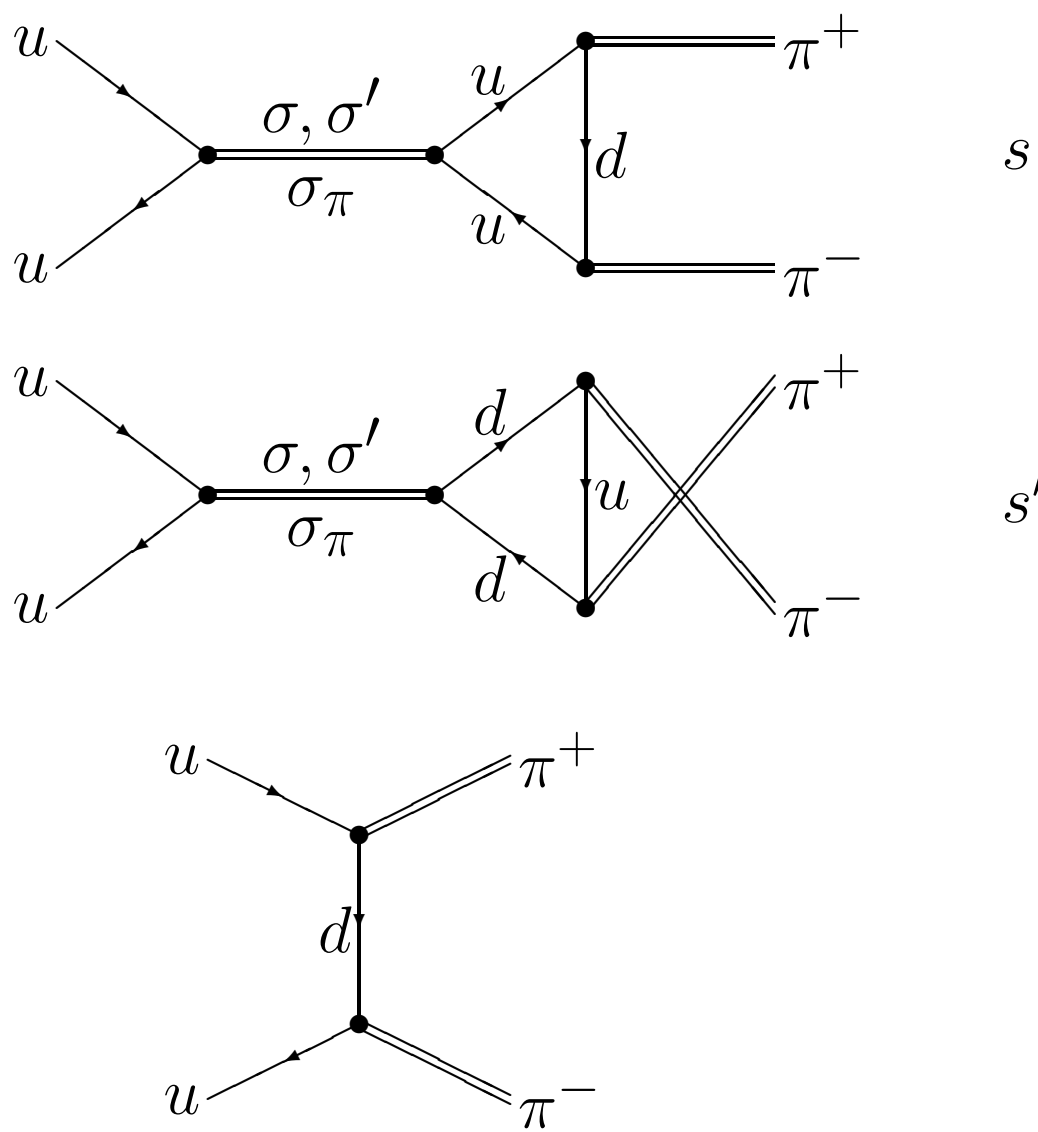


Figure 11